Human OTULIN haploinsufficiency impairs cell-intrinsic immunity to staphylococcal alpha-toxin

Spaan, Andras N.

2022-06-17

Human OTULIN haploinsufficiency impairs cell-intrinsic immunity to staphylococcal α-toxin

András N. Spaan[1,2]*, Anna-Lena Neehus[3,4,5]†, Emmanuel Laplantine[6,7]†, Frederik Staels[8]†, Masato Ogishi[1]†, Yoann Seeleuthner[3,4]†, Franck Rapaport[1]†, Keenan A. Lacey[9], Erika Van Nieuwenhove[8,10], Maya Chrabieh[3,4], David Hum[1], Mélanie Migaud[3,4], Araksya Izmiryan[4,11], Lazaro Lorenzo[3,4], Tatiana Kochetkov[1], Dani A. C. Heesterbeek[2], Bart W. Bardoel[2], Ashley L. DuMont[9], Kerry Dobbs[12], Solenne Chardonnet[13], Søren Heissel[14], Timour Baslan[15], Peng Zhang[1], Rui Yang[1], Dusan Bogunovic[16], Herman F. Wunderink[2], Pieter-Jan A. Haas[2], Henrik Molina[14], Griet Van Buggenhout[17,18], Stanislas Lyonnet[4,19], Luigi D. Notarangelo[12], Mikko R. J. Seppänen[20], Robert Weil[6], Gisela Seminario[21], Héctor Gomez-Tello[22], Carine Wouters[8,23], Mehrnaz Mesdaghi[24], Mohammad Shahrooei[25,26], Xavier Bossuyt[25], Erdal Sag[27], Rezan Topaloglu[28], Seza Ozen[27], Helen L. Leavis[29], Maarten M. J. van Eijk[30], Liliana Bezrodnik[21], Lizbeth Blancas Galicia[31], Alain Hovnanian[4,11,32], Aude Nassif[33], Brigitte Bader-Meunier[4,34,35], Bénédicte Neven[4,34,35], Isabelle Meyts[36,37], Rik Schrijvers[38], Anne Puel[1,3,4], Jacinta Bustamante[1,3,4,39], Ivona Aksentijevich[40], Daniel Kastner[40], Victor J. Torres[9], Stéphanie Humblet-Baron[8]‡, Adrian Liston[8,41,42]‡, Laurent Abel[1,3,4]‡, Bertrand Boisson[1,3,4]§, Jean-Laurent Casanova[1,3,4,43,44]*§

[1]St. Giles Laboratory of Human Genetics of Infectious Diseases, Rockefeller Branch, The Rockefeller University, New York, NY 10065, USA. [2]Department of Medical Microbiology, University Medical Center Utrecht, Utrecht University, 3584 CX Utrecht, Netherlands. [3]Laboratory of Human Genetics of Infectious Diseases, Necker Branch, INSERM U1163, Necker Hospital for Sick Children, 75015 Paris, France. [4]Paris Cité University, Imagine Institute, 75015 Paris, France. [5]Institute of Experimental Hematology, REBIRTH Research Center for Translational and Regenerative Medicine, Hannover Medical School, 30625 Hannover, Germany. [6]Sorbonne University, INSERM U1135, CNRS ERL8255, Centre d'Immunologie et des Maladies Infectieuses, 75724 Paris, France. [7]Paris Cité University, Institut de Recherche St. Louis, Hôpital St. Louis, INSERM U944, CNRS U7212, 75010 Paris, France. [8]Laboratory for Adaptive Immunology, Department of Microbiology, Immunology and Transplantation, KU Leuven, 3000 Leuven, Belgium. [9]Department of Microbiology, New York University Grossman School of Medicine, New York, NY 10016, USA. [10]Department of Pediatric Rheumatology and Immunology, Wilhelmina Children's Hospital, University Medical Center Utrecht, Utrecht University, 3584 CX Utrecht, Netherlands. [11]Laboratory of Genetic Skin Diseases, INSERM U1163, 75015 Paris, France. [12]Laboratory of Clinical Immunology and Microbiology, Division of Intramural Research, NIAID, NIH, Bethesda, MD 20852, USA. [13]Sorbonne University, INSERM, UMS Production et Analyse de données en Sciences de la vie et en Santé, PASS, Plateforme Post-génomique de la Pitié-Salpêtrière, P3S, 75013 Paris, France. [14]Proteomics Resource Center, The Rockefeller University, New York, NY 10065, USA. [15]Cancer Biology and Genetics Program, Memorial Sloan Kettering Cancer Center, New York, NY 10065, USA. [16]Icahn School of Medicine at Mount Sinai, New York, NY 10029, USA. [17]Department of Human Genetics, KU Leuven, 3000 Leuven, Belgium. [18]Center for Human Genetics, University Hospitals Leuven, 3000 Leuven, Belgium. [19]Laboratory Embryology and Genetics of Malformations, INSERM U1163, Necker Hospital for Sick Children, 75015 Paris, France. [20]Rare Disease and Pediatric Research Centers, Children and Adolescents, University of Helsinki and HUS Helsinki University Hospital, 00260 Helsinki, Finland. [21]Center for Clinical Immunology, Immunology Group Children's Hospital Ricardo Gutiérrez, C1425EFD Buenos Aires, Argentina. [22]Poblano Children's Hospital, Immunology Department, 72190 Puebla, Mexico. [23]Department of Pediatrics, University Hospitals Leuven, 3000 Leuven, Belgium. [24]Department of Allergy and Clinical Immunology, Mofid Children's Hospital, Shahid Beheshti University of Medical Sciences, 15468-155514 Tehran, Iran. [25]Clinical and Diagnostic Immunology, Department of Microbiology, Immunology and Transplantation, KU Leuven, 3000 Leuven, Belgium. [26]Specialized Immunology Laboratory of Dr. Shahrooei, Sina Medical Complex, 15468-155514 Ahvaz, Iran. [27]Department of Pediatric Rheumatology, Hacettepe University, 06230 Ankara, Turkey. [28]Department of Pediatric Nephrology, Hacettepe University, 06230 Ankara, Turkey. [29]Department of Rheumatology and Clinical Immunology, University Medical Center Utrecht, Utrecht University, 3584 CX Utrecht, Netherlands. [30]Department of Intensive Care Medicine, University Medical Center Utrecht, Utrecht University, 3584 CX Utrecht, Netherlands. [31]Immune Deficiencies Laboratory National Institute of Pediatrics, 04530 Mexico City, Mexico. [32]Department of Genetics, Necker Hospital for Sick Children, AP-HP, 75015 Paris, France. [33]Centre Médical, Institut Pasteur, 75724 Paris, France. [34]Pediatric Immunology, Hematology and Rheumatology Unit, Necker Hospital for Sick Children, AP-HP, 75015 Paris, France. [35]Laboratory of Immunogenetics of Pediatric Autoimmunity, INSERM U1163, Necker Hospital for Sick Children, 75015 Paris, France. [36]Laboratory of Inborn Errors of Immunity, Department of Microbiology, Immunology and Transplantation, KU Leuven, 3000 Leuven, Belgium. [37]Department of Pediatrics, Jeffrey Modell Diagnostic and Research Network Center, University Hospitals Leuven, 3000 Leuven, Belgium. [38]Allergy and Clinical Immunology Research Group, Department of Microbiology, Immunology and Transplantation, KU Leuven, 3000 Leuven, Belgium. [39]Study Center for Primary Immunodeficiencies, Necker Hospital for Sick Children, AP-HP, 75015 Paris, France. [40]Inflammatory Disease Section, National Human Genome Research Institute, Bethesda, MD 20892, USA. [41]VIB Center for Brain and Disease Research, Leuven 3000, Belgium. [42]Immunology Programme, Babraham Institute, Babraham Research Campus, Cambridge CB22 3AT, UK. [43]Department of Pediatrics, Necker Hospital for Sick Children, AP-HP, 75015 Paris, France. [44]Howard Hughes Medical Institute, The Rockefeller University, New York, NY 10065, USA.

†These authors contributed equally to this work.

‡These authors contributed equally to this work.

§These authors contributed equally to this work.

*Corresponding author. Email: a.n.spaan@umcutrecht.nl (A.N.S); casanova@rockefeller.edu (J.-L.C.)

The molecular basis of interindividual clinical variability upon infection with *Staphylococcus aureus* is unclear. We describe patients with haploinsufficiency for the linear deubiquitinase OTULIN, encoded by a gene on chromosome 5p. Patients present episodes of life-threatening necrosis, typically triggered by *S. aureus* infection. The disorder is phenocopied in patients with the 5p- (Cri-du-Chat) chromosomal deletion syndrome. OTULIN haploinsufficiency causes an accumulation of linear ubiquitin in dermal fibroblasts, but TNF-receptor NF-κB-signaling remains intact. Blood leukocyte subsets are unaffected. The OTULIN-dependent accumulation of caveolin-1 in dermal fibroblasts—but not leukocytes—facilitates the cytotoxic damage inflicted by the staphylococcal virulence factor α-toxin. Naturally elicited antibodies against α-toxin contribute to incomplete clinical penetrance. Human OTULIN haploinsufficiency underlies life-threatening staphylococcal disease by disrupting cell-intrinsic immunity to α-toxin in non-leukocytic cells.

Staphylococcus aureus is a major bacterial pathogen with a global impact on human health (*1*). Individuals with staphylococcal disease may present a range of superficial (folliculitis, cellulitis, abscesses) to severe (e.g., necrotizing skin and soft tissue infections and necrotizing pneumonia, with or without septicemia) manifestations (*1*). Most individuals carry *S. aureus* asymptomatically on their skin and in their nostrils for long periods of their lives, but only a minority develop life-threatening staphylococcal disease. Severe disease has a poor prognosis, owing to its rapid invasive course (*2–5*). Acquired risk factors for staphylococcal disease include surgery and intravascular devices (*1*). Life-threatening staphylococcal disease can also result from single-gene inborn errors of immunity (IEIs) (*6*). Disorders affecting phagocyte development or function, such as severe congenital neutropenia, chronic granulomatous disease, and leukocyte adhesion deficiency, confer a predisposition to staphylococcal disease (*6, 7*). Disorders of the Toll-like receptor (TLR) and interleukin (IL)-1R nuclear factor-kappa B (TIR-NF-κB) pathway (*8–12*) and of IL-6- and STAT3-dependent immunity (*13–17*) have also been identified in patients suffering from severe staphylococcal disease. All these defects preferentially affect innate, myeloid immunity, but, collectively, they account for only a small proportion of cases (*18*). Most cases of severe staphylococcal disease remain unexplained, because they strike otherwise healthy individuals with no detectable phagocyte defect (*2, 19*). Here, we aimed to elucidate human genetic and immunological etiologies of life-threatening staphylococcal disease.

Results

Genome-wide enrichment in rare *OTULIN* variants

Given the severity of their disease, we hypothesized that there would be at least some genetic homogeneity in our cohort of patients with unexplained life-threatening staphylococcal disease. We sequenced the exomes of the N = 105 index cases. Given the rarity of severe staphylococcal disease in otherwise healthy individuals, and assuming a dominant mode of inheritance, we hypothesized that the disease-causing variants

would be very rare [minor allele frequency (MAF) < 1×10^{-5}] (*20*). We also prioritized variants predicted to be deleterious [combined annotation-dependent depletion score (CADD) > mutation significance cutoff (MSC)] (*21–23*). We performed the same analysis on N = 1,274 control exomes from patients with mycobacterial diseases (including individuals with Mendelian susceptibility to mycobacterial disease or with tuberculosis), which rarely overlap with staphylococcal disease (*24*). After adjusting for ethnicity by principal component analysis (PCA), we used the results of these two analyses to test the null hypothesis that variants of a given gene were not specific to staphylococcal disease. *OTULIN* was the only gene satisfying the threshold for statistical significance on a genome-wide level with a P-value of 5.74×10^{-7} (Fig. 1A and tables S1 and S2). We repeated our analysis for *OTULIN,* adding 2,504 individuals from the 1,000 Genomes Project (*25*) to our control dataset (*26*); none of these individuals had developed life-threatening infections with *S. aureus*. The enrichment in *OTULIN* variants was even stronger (P = 3.85×10^{-8}) in this analysis, indicating that very rare variants of this gene were found specifically in patients with severe staphylococcal disease.

The patients carry heterozygous *OTULIN* variants

The linear deubiquitinase OTULIN is a negative regulator of inflammation (*27, 28*). In humans, biallelic *OTULIN* mutations cause a potentially fatal early-onset autoinflammatory condition called OTULIN-related autoinflammatory syndrome (ORAS) (*29–33*). Closer inspection revealed that the signal for genetic homogeneity in the cohort of patients with severe staphylococcal disease was driven by three probands carrying heterozygous variants of *OTULIN* (Fig. 1B): one missense (p.D246V), one nonsense (p.E95X), and one frameshift (p.D268TfsX5) variant. In each of these probands, the clinical hallmark of disease following infection with *S. aureus* was life-threatening necrosis of the skin and/or lungs [fig. S1A; supplementary materials (SM)]. Based on the extreme inflammatory responses to infection with *S. aureus* in these patients, we investigated the possibility of other triggers

generating similar disease. We identified three additional kindreds with very rare heterozygous missense variants of *OTULIN* (p.N341D, p.P254S, and p.R263Q) (Fig. 1C). The probands of these kindreds presented severe diseases triggered by infectious and unknown etiologies (fig. S1B; SM). The clinical course of disease in patients with no documented infection suggests that low-grade infections, or non-infectious triggers, might induce an inflammatory phenotype similar to that of patients with documented *S. aureus* infection (fig. S1, A and B; SM). In total, we identified six very rare variants in seven patients from six kindreds (fig. S1C). These seven patients did not carry variants fitting the known modes of inheritance for any of the 430 genes already implicated in IEIs (*7*, *34*). In most patients, the first episode of disease occurred during adolescence (SM). Clinical data indicated a degree of phenotypic heterogeneity in the index cases, but with the skin and/or lungs consistently affected in all cases (Fig. 1, B and C, and fig. S1, A and B; SM). One third of the heterozygous relatives (three of the nine for whom data were available) expressed a related but milder phenotype, the other six carriers being apparently healthy (Fig. 1, B and C; SM). We then hypothesized that the parents of the patients with biallelic OTULIN deficiency reported in previous studies (*29–32*), who themselves carried deleterious *OTULIN* alleles in the heterozygous state, might present phenocopies of the disorder observed in the patients of our cohort. One third of the parents (three of the 10) did, indeed, express the phenotype (Fig. 1D; SM). Thus, very rare heterozygous mutations of *OTULIN* confer predisposition to severe necrosis of the skin and lungs, typically, but not exclusively, after infection with *S. aureus*, with variable expressivity and incomplete penetrance.

OTULIN is subject to negative selection

The severity of disease in the probands carrying very rare heterozygous *OTULIN* variants suggests that this gene is subject to evolutionary forces acting at the population level. Indeed, the f parameter score for *OTULIN* is 0.36, indicating that this gene is under negative selection (fig. S1D) (*35*). Moreover, the consensus score for negative selection (CoNeS) for *OTULIN* is −0.78, within the reported range for genes underlying IEIs with both autosomal dominant (AD) and autosomal recessive (AR) inheritance (fig. S1E) (*36*). *OTULIN* has a LoFtool score of 0.115, suggesting that it does not tolerate haploinsufficiency (*37*). Predicted loss-of-function (pLOF) *OTULIN* variants are very rare in the general population, with a cumulative MAF of 1×10^{-4} (fig. S1F) (*20*). Consistent with the negative selection pressure acting on *OTULIN*, the alleles of the patients were found to be either ultra-rare or private (fig. S1F) (*20*). These population genetics parameters indicate that heterozygous pLOF variants of *OTULIN* are disadvantageous for the individual. This finding is consistent with the hypothesis that the very rare variants for which enrichment was

detected in the patients studied are causal for the life-threatening necrosis of the skin and/or lungs triggered by *S. aureus* infection.

The OTULIN alleles of the patients are severely hypomorphic or amorphic

We overexpressed the cDNAs corresponding to the *OTULIN* alleles of the patients in HEK293T cells. The truncated cDNAs of the patients were loss-of-expression, whereas the missense cDNAs of the patients and cDNAs corresponding to two *OTULIN* alleles commonly found in the general population (*20*) were expressed at normal levels (fig. S1G). No in-frame re-initiation was observed for truncated alleles from the patients (fig. S1H). We then assessed the deubiquitinase activity of the products of the alleles from the patients, and their capacity to inhibit NF-κB-signaling. Consistent with published findings in overexpression systems, some, but not all the protein products of the alleles concerned were defective for the linear deubiquitination of NEMO in the presence of LUBAC (fig. S1I) (*32*, *33*). We assessed the capacity of the gene products to regulate receptor signaling, by investigating the functional consequences of the *OTULIN* alleles of the patients for NF-κB inhibition following stimulation with TNF in a cellular signaling system. All the alleles from patients were severely hypomorphic or amorphic (fig. S1J). By contrast to the alleles of the patients, the two alleles common in the general population (*20*) were found to be isomorphic (fig. S1J). The apparent differences between the two overexpression systems may reflect different impacts of the various OTULIN alleles on ubiquitin binding capacity (*27*, *32*, *33*). We then performed functional tests for all the other *OTULIN* coding sequence variants reported in public databases (N = 120) (*20*). The cumulative MAF of amorphic and hypomorphic *OTULIN* alleles (with <25% wild-type levels of NF-κB-signaling inhibitory activity) in the general population was 6×10^{-5} (Fig. 1E). The greater rarity of amorphic and hypomorphic *OTULIN* alleles than of pLOF variants highlights the importance of experimental validation for pLOF variants. Thus, the rare *OTULIN* variants found in the patients are deleterious and AD OTULIN deficiency predisposes the patients to disease.

Autosomal dominant OTULIN deficiency acts via haploinsufficiency

We tested the genetic mechanism of AD OTULIN deficiency and found no negative dominance for the alleles expressed by the patients (fig. S1K). This implies that the genetic mechanism underlying AD OTULIN deficiency is haploinsufficiency. *OTULIN* is located on the short arm of chromosome 5. Depending on the breakpoint, almost all individuals with 5p- syndrome—the most common chromosomal deletion syndrome in humans, also known as Cri-du-Chat syndrome—are haploinsufficient for OTULIN by definition (*38–40*). The

prevalence of 5p- syndrome is ~1 in 50,000 live births, similar to the cumulative MAF for amorphic and hypomorphic *OTULIN* alleles (Fig. 1E) (*41*). Respiratory tract infections are one of the principal causes of hospitalization in individuals with 5p- syndrome, and pneumonia is amongst the commonest causes of death in these individuals (*40, 42–44*). We recruited six 5p- syndrome patients with a breakpoint centromeric to *OTULIN* (Fig. 1F and fig. S1L). Expressivity was variable and penetrance was incomplete, but one third of these OTULIN haploinsufficient 5p- syndrome patients (two of six) presented an age-dependent phenocopy of the disorder observed in patients with heterozygous *OTULIN* mutations (Fig. 1F; SM). We also identified two individuals from a multigeneration kindred affected by 5p- syndrome with an extremely rare breakpoint telomeric to *OTULIN* (Fig. 1G and fig. S1L) (*38*). Both these individuals carried two copies of *OTULIN* and did not display the phenotype studied here (SM). The clinical similarities between patients with heterozygous *OTULIN* mutations and those with 5p- syndrome suggest a common mechanism of predisposition to infection due to haploinsufficiency for OTULIN.

Immunological characterization of OTULIN-haplo-insufficient PBMCs

The autoinflammatory features seen in ORAS patients are largely driven by abnormally high levels of NF-κB activation in myeloid cells (*29, 30, 33*). We thus investigated whether patients with OTULIN haploinsufficiency presented any related immunological disturbances. OTULIN expression in monocytes differed between patients and healthy controls (fig. S2A). Routine immunological tests performed in diagnostic laboratories [including assessments of leukocyte differentiation and oxidative burst capacity—deficiencies of which are known to confer a predisposition to staphylococcal disease (*6, 7*)] revealed no explanatory defects in patients with OTULIN haploinsufficiency (SM). We thus looked for more subtle immunological features, by testing PBMCs from the patients by mass cytometry (cytometry by time-of-flight, CyTOF) (*45*) and RNA sequencing. In comparisons with healthy controls, we observed no differences in the abundance of leukocyte subsets or in the expression of lineage markers (Fig. 2A and fig. S2, B to D). The development of myeloid and lymphoid subsets in patients with OTULIN haploinsufficiency was, therefore, apparently normal. At baseline, we observed a complex transcriptional signature not associated with NF-κB-driven inflammation in the PBMCs of the patients (Fig. 2B and fig. S2E). This difference between the patients and healthy controls disappeared following stimulation (Fig. 2B). Both at baseline and after stimulation, the PBMCs of the patients had a capacity to secrete various cytokines, including TNF and IL-1β, similar to that of PBMCs from healthy controls (fig. S2F). We detected no

defect of IL-6 production (fig. S2F), deficiencies of which are known to be associated with staphylococcal disease (*6*). Single-cell RNA sequencing revealed a contribution of CD14+ monocytes to the transcriptional signature in the PBMCs of the patients relative to healthy controls (fig. S2, G and H). However, consistent with their capacity to produce normal amounts of TNF and IL-1β (fig. S2I), the amounts of phosphorylated P65 in CD14+ monocytes from the patients were normal both at baseline and following stimulation (fig. S2J). The CD14+ monocytes of patients with OTULIN haploinsufficiency, thus, did not appear to be functionally affected. Finally, induced pluripotent stem cell (iPSC)–derived macrophages from patients had normal oxidative burst and phagocytic capacities relative to healthy controls (fig. S2, K and L). These observations suggest an absence of overt immunological disturbance in patients with OTULIN haploinsufficiency, contrasting with the autoinflammatory markers described in ORAS patients (*29–33*).

OTULIN gene dosage-dependent accumulation of linear ubiquitin in fibroblasts

We next performed a biochemical characterization of the non-hematopoietic compartment in the patients and assessed the levels of *OTULIN* expression in primary dermal fibroblasts (PDFs). *OTULIN* mRNA levels varied (fig. S3, A and B), but the levels of the corresponding protein were low in the patients and depended on the nature of the mutation (Fig. 3, A and B). OTULIN haploinsufficiency led to an accumulation of aggregates containing linear ubiquitin (M1-Ub) in immortalized fibroblasts from patients, including 5p- syndrome patients with a breakpoint centromeric to *OTULIN* (Fig. 3, C and D, and fig. S3C). These aggregates were sensitive to treatment with exogenous OTULIN (fig. S3D), and their accumulation was rescued by genetic complementation with wild-type *OTULIN* (Fig. 3E and fig. S3E). We used a combination of an M1-Ub-selective tandem Ub-binding entity (TUBE) and absolute quantification (AQUA) tandem mass spectrometry (MS/MS) to assess M1-Ub levels in immortalized fibroblasts from the patients. M1-Ub levels were much higher in the cells of both ORAS and OTULIN-haploinsufficient patients than in those of healthy controls and HOIL1-deficient patients (Fig. 3F) (*46*). Thus, OTULIN haploinsufficiency and recessive deficiency result in the cellular accumulation of M1-Ub in a gene dosage-dependent manner.

Normal TNF-receptor signaling in OTULIN-haplo-insufficient fibroblasts

In the PDFs of ORAS patients, expression of the components of the linear ubiquitin assembly complex (LUBAC) decreases to compensate for recessive OTULIN deficiency (Fig. 3A) (*29, 30, 32*). This compensatory mechanism impaired TNF-receptor signaling in immortalized fibroblasts from ORAS

patients (fig. S3F). By contrast, OTULIN haploinsufficiency did not lead to a loss of LUBAC expression in PDFs (Fig. 3A), or to impaired TNF-receptor signaling (fig. S3F) or IL-6 and IL-8 secretion (fig. S3G). Indeed, no differential transcription patterns were evident in the patients' PDFs after stimulation with TNF (fig. S3H). The impairment of early NF-κB activation sensitizes PDFs from ORAS and LUBAC-deficient patients to TNF-induced apoptotic cell death under stress conditions (*29*, *46*). However, consistent with their normal LUBAC expression, PDFs from patients with OTULIN haploinsufficiency were not susceptible to stress-induced apoptosis upon exposure to TNF (fig. S3I). Thus, the functional dysregulation of TNF-receptor signaling via NF-κB is limited to fibroblasts displaying a recessive OTULIN deficiency.

Global dysregulation of transcription in OTULIN-haploinsufficient fibroblasts

The presence of a biochemical phenotype in the absence of an immunological phenotype following stimulation in OTULIN-haploinsufficient fibroblasts led us to investigate transcriptional homeostasis in resting PDFs from the patients. Consistent with the gene dosage-dependent accumulation of M1-Ub in immortalized fibroblasts, this approach revealed a continuous genotype-dependent transcriptional phenotype in the basal state (Fig. 4A). Despite an absence of functional consequences of OTULIN haploinsufficiency (fig. S3, F to I), specific gene-set enrichment analyses of the resting transcriptome revealed a subtle signal for TNF-receptor signaling via NF-κB (fig. S4A). These analyses also revealed a transcriptional signature affecting various other cellular processes relative to cells from healthy controls (fig. S4A) (*47*). The affected processes included the MYC and E2F transcription factor systems and the G2M cell cycle checkpoint system, the gene sets for these systems displaying a partial overlap (fig. S4B). These findings indicate a global dysregulation of transcription in resting OTULIN-haploinsufficient fibroblasts.

Accumulation of caveolin-1 in OTULIN-haploinsufficient fibroblasts

The observed patterns of transcription could not be explained by the known function of OTULIN as a linear deubiquitinase. We thus hypothesized that OTULIN haploinsufficiency affects cellular homeostasis posttranslationally, in an as yet unknown manner. The proteome of the resting PDFs from the patients displayed a continuous cellular phenotype, consistent with the transcriptome (Fig. 4B and fig. S4C). Focusing on this continuous proteomic phenotype, we observed a pattern of differential abundance for a cluster of 11 proteins including caveolin-2 and gelsolin (fig. S4, D to F). A STRING-interaction network analysis of this protein cluster identified a node connecting caveolin-2 and gelsolin: caveolin-1 (Fig.

4C). Conventional techniques revealed the accumulation of SDS-resistant high-molecular weight (MW) caveolin-1-containing complexes (*48*, *49*) in PDFs from the patients in comparison with those from healthy controls (Fig. 4, D and E). We analyzed caveolin-1 immunopurification products (IPs) from PDF whole-cell lysates (WCLs) from one healthy control and one patient with recessive OTULIN deficiency by liquid chromatography and tandem mass spectrometry (LC-MS/MS). Validating the STRING-interaction network (Fig. 4C), both sets of caveolin-1 IPs also contained caveolin-2, whereas gelsolin was detected in the OTULIN-deficient sample only (fig. S4G). Caveolin-1 levels vary between cell types and are highest in structural cells, such as fibroblasts (*50*, *51*). By contrast to our observations for PDFs, caveolin-1 was barely detectable in hematopoietic cells and the abundance of caveolin-1 in monocytes did not differ between OTULIN haploinsufficient patients and healthy controls (fig. S4H). We detected no accumulation of caveolin-1-containing complexes in PDFs from the 5p- syndrome patient carrying two copies of the *OTULIN* gene relative to healthy controls (Fig. 4E and fig. S4I). However, as in PDFs from the patients, caveolin-1 accumulated as a high-MW complex in an isogenic *OTULIN*-knockout PDF cell line (Fig. 4F and fig. S4J). Thus, OTULIN haploinsufficiency results in a selective accumulation of high-MW caveolin-1 in PDFs.

Lysine-63-linked polyubiquitination of caveolin-1

The differences in gelsolin abundance in PDFs were attributed to differences in *GSN* transcription, but no differential transcription was detected for *CAV1* and *CAV2* (fig. S5A). Caveolin-1 is a key component of cell membrane microdomains, in which it acts as a scaffold for other proteins and receptors (*47*, *52*). A signal for plasma membrane disturbance was detected at the proteomic but not transcriptional level in the patients' PDFs (fig. S5B), suggesting a post-translational role for OTULIN in the regulation of caveolin-1 expression in PDFs. Caveolin-1 is decorated with ubiquitin (*48*, *49*, *53*). We hypothesized that OTULIN haploinsufficiency and recessive deficiency affect the ubiquitination status of caveolin-1. We found that caveolin-1 IPs from PDF-WCLs from one healthy control and one patient with recessive deficiency of OTULIN contained a high-MW ubiquitin-containing complex (fig. S5C). We then used LC-MS/MS to characterize the ubiquitination profiles of purified caveolin-1 in solution, in the high-MW complex fraction, and in the monomeric fraction. Lysine-48-linked polyubiquitin (K48-Ub) chains were conjugated to the high-MW caveolin-1-containing complex regardless of genotype (fig. S5D). We detected no M1-Ub in any of the caveolin-1 IP fractions (fig. S5, C and D). Instead, the high-MW caveolin-1-containing complex was abundantly decorated with lysine-63-linked polyubiquitin (K63-Ub) chains in the OTULIN-deficient sample, but not in the healthy control

(Fig. 5A and fig. S5C) (*49*). No other branched polyubiquitin linkages were detected in the caveolin-1 IP fractions. The remaining unmodified ubiquitin was probably conjugated as a monomer to caveolin-1 (fig. S5D) (*53*). The OTULIN-dependent accumulation of caveolin-1 complexes modified with K63-Ub but not M1-Ub chains indicates crosstalk between OTULIN and other ubiquitin ligases and/or hydrolases.

CYLD binds linear ubiquitin

We characterized the crosstalk between OTULIN and K63-Ub chains, by treating purified caveolin-1 from one ORAS patient with a panel of recombinant deubiquitinases. Consistent with the respective specificities of the various hydrolases, the K63-linked polyubiquitination of high-MW caveolin-1 was reduced by treatment with recombinant CYLD but not OTULIN (Fig. 5B and fig. S5E). Similarly, the overexpression of *CYLD* but not *OTULIN* in PDFs from a patient with ORAS rescued the K63-linked polyubiquitination of high-MW caveolin-1 (Fig. 5C and fig. S5F). Unexpectedly, a stronger rescue was observed when both *CYLD* and *OTULIN* were overexpressed (Fig. 5C and fig. S5F). Caveolin-1 colocalized with K63-Ub and, to some extent, with M1-Ub aggregates in PDFs (fig. S5G). We used a combination of TUBE and high-input AQUA-MS/MS in immortalized fibroblasts to identify proteins bound to M1-Ub. We detected LUBAC components (fig. S5H), which are known to be decorated with M1-Ub (*29*). We also identified caveolin-1 and CYLD as possibly binding to M1-Ub fig. S5H), and used cells from a HOIL1-deficient patient to validate specificity (*46*). The detection of caveolin-1 was not specific (fig. S5I), consistent with the absence of M1-Ub in the caveolin-1 IP (Fig. 5A and fig. S5, C and D). We confirmed the specific binding of CYLD to M1-Ub in an *OTULIN* gene-dosage dependent manner (Fig. 5D and fig. S5I). The M1-Ub-bound CYLD-species had a higher MW than that for the total CYLD-pool (fig. S5I), suggesting posttranslational modification. We identified no Gly-Gly ubiquitination signature sites on CYLD by proteomic approaches, suggesting that the post-translational modification is not ubiquitination itself and that the binding of CYLD to M1-Ub is non-covalent. Unlike an *OTULIN* gene-dosage effect, M1-Ub-bound HOIP was detected in cells from ORAS patients only (Fig. 5D fig. S5, I and J). These data reveal a direct, LUBAC-independent but OTULIN-dependent binding of M1-Ub to CYLD.

Colocalization of caveolin-1 with S. aureus α-toxin

Caveolin-1 clusters in membrane microdomains (*52*) and has been reported to colocalize with a disintegrin and metallo-protease domain-containing protein 10 (ADAM10) (*54*). ADAM10 is a cell surface receptor used by the staphylococcal virulence factor α-toxin (*54, 55*). α-Toxin is a pore-forming cytotoxin triggering ADAM10-mediated cell death in a process facilitated by caveolin-1 (*56*). We hypothesized that the OTULIN-dependent caveolin-1 accumulation in the PDFs from the patients would contribute to the adverse outcomes of their disease. We thus investigated the cellular kinetics of α-toxin binding. Following its addition to PDFs, α-toxin colocalized with both ADAM10 and caveolin-1 (Fig. 6A and fig. S6, A and B). ADAM10 and caveolin-1 were colocalized to some extent in the presence or absence of toxin binding (Fig. 6A and fig. S6, A and B). The patients' PDFs displayed moderately higher levels of α-toxin binding than cells from healthy controls (Fig. 6B and fig. S6C). This observation could not be explained by differential ADAM10 expression at baseline (fig. S6, D and E). However, after α-toxin binding, the expression of ADAM10 at the cell surface was greater in PDFs from patients than in those from healthy controls (fig. S6F). These data suggest a role for caveolin-1 in retaining ADAM10 at the surface of the cell when OTULIN-haploinsufficient fibroblasts are exposed to α-toxin (*57, 58*).

OTULIN haploinsufficiency impairs intrinsic immunity to α-toxin

We hypothesized that OTULIN haploinsufficiency confers a predisposition to α-toxin-induced cell death in the PDFs of the patients. Indeed, these cells displayed an enhanced susceptibility to *S. aureus* culture supernatant-elicited cytotoxicity (Fig. 6C). This cytotoxicity was antagonized by prior treatment of the supernatant with α-toxin-neutralizing monoclonal antibodies (fig. S6G), indicating a major contribution of α-toxin to cytotoxicity in these cells. *OTULIN* genotype-dependent susceptibility to α-toxin was confirmed with recombinant α-toxin (Fig. 6D and fig. S6H). The absence of a particular phenotype following the treatment of cells from patients with streptolysin O (SLO) and aerolysin—microbial toxins produced by other bacteria and not requiring specific proteinaceous host-cell surface receptors (*59*)—indicates a specific susceptibility of the OTULIN-haploinsufficient PDFs from patients to α-toxin (Fig. 6D and fig. S6H). Normal susceptibility to α-toxin was observed in PDFs from a 5p- syndrome patient carrying two copies of the *OTULIN* gene, confirming the OTULIN-dependence of the phenotype (Fig. 6E and fig. S6I). α-Toxin elicited higher levels of cell surface metalloprotease activation in PDFs from the patients than in those of healthy controls (Fig. 6F) (*55*). Again, a 5p- syndrome patient carrying two copies of the *OTULIN* gene behaved like controls (Fig. 6F). Activity levels were correlated with ADAM10 levels following α-toxin binding (fig. S6J). Prior treatment of the PDFs with an ADAM10-selective inhibitor blocked α-toxin-induced metalloprotease activation completely in controls, but activation levels in patients were decreased only slightly, to those in untreated controls (Fig. 6F). Moreover, to various extents, ADAM10 inhibition protected the patients' PDFs against α-toxin cytotoxicity (fig. S6K).

Prior treatment with cyclodextrin, a chemical product disrupting caveolin-1-enriched membrane microdomains (*60*), protected PDFs from the patients against α-toxin-induced cytotoxicity (fig. S6K). The susceptibility of an OTULIN-deficient PDF cell line was partially rescued by knocking out *CAV1* but not *CAV2* (Fig. 6G and fig. S6L), further supporting a facilitating role of caveolin-1 in α-toxin cytotoxicity (*54*). Consistent with the low levels of caveolin-1 in hematopoietic cells from the patients, these cells displayed no OTULIN-dependent susceptibility to α-toxin (fig. S6M). Murine PDFs, unlike their human counterparts, were resistant to α-toxin-elicited cell death regardless of *Otulin* genotype (fig. S6N). Thus, OTULIN haploinsufficiency results in a human-specific cell-intrinsic susceptibility of non-hematopoietic cells to the major *S. aureus* virulence factor, α-toxin.

α-Toxin-neutralizing antibodies rescue OTULIN haploinsufficiency

Colonization and infection with *S. aureus* elicit α-toxin-neutralizing antibodies in an age-dependent manner (*61*). We hypothesized that α-toxin-neutralizing antibodies in the plasma of adult symptomatic and asymptomatic heterozygotes might contribute to the incomplete clinical penetrance of OTULIN haploinsufficiency (Fig. 1, B to D and F) (*12*). Routine measurements of immunoglobulin levels and vaccine responses revealed no defects in the patients (SM). Plasma α-toxin-neutralizing capacity in asymptomatic carriers was similar to that of healthy controls, whereas this capacity was significantly lower in patients (~one fifth that in healthy controls; Fig. 7A and fig. S7A). The lower neutralizing capacity in the patients was specific for α-toxin, because the plasma of the patients neutralized SLO and pneumolysin normally (Fig. 7A and fig. S7A). In healthy controls, plasma α-toxin-neutralizing capacity was largely driven by IgG (fig. S7B). In patients, anti-α-toxin IgG levels were significantly lower than those in healthy controls, whereas IgA and IgM levels were unaffected (Fig. 7B and fig. S7, C and D). The anti-α-toxin IgG levels in asymptomatic carriers were like those of healthy controls (Fig. 7B and fig. S7, C and D) (*61*). Similar observations were made following correction for sample-specific total IgG levels (fig. S7E). Thus, naturally elicited α-toxin-neutralizing antibodies can rescue OTULIN haploinsufficiency in vivo, thereby contributing to incomplete penetrance.

Discussion

We tested the hypothesis that some patients from our cohort with severe staphylococcal disease suffered from IEIs. Using an unbiased approach, we detected a genome-wide enrichment in very rare, deleterious heterozygous *OTULIN* variants in the cohort. We identified haploinsufficiency for OTULIN as a genetic etiology of severe staphylococcal disease. AR OTULIN deficiency results in life-threatening autoinflammation, manifesting early in life as ORAS (*29–32*). By contrast, patients with AD OTULIN deficiency typically presented with severe disease triggered by *S. aureus* infections. Most of the patients with OTULIN haploinsufficiency experienced their first episode of disease during adolescence. Necrosis was a clinical hallmark of disease in the probands. Some patients were not diagnosed with *S. aureus* infections, suggesting that low-grade infectious or, perhaps, non-infectious triggers might be at work. AD OTULIN deficiency is clinically expressed in a tissue-specific manner because the skin and/or lungs are the affected organs in all patients. The pedigrees reported in our study displayed variable degrees of penetrance and expressivity. Such observations are common in situations of haploinsufficiency (*62, 63*). We show that naturally elicited α-toxin-neutralizing antibodies can rescue OTULIN haploinsufficiency and we suspect that declining levels of such antibodies may contribute to recurrent episodes of severe staphylococcal disease in some patients. We estimate the clinical penetrance of AD OTULIN deficiency at about 30%. This estimate of clinical penetrance mirrors our findings for individuals with 5p- syndrome. It is difficult to establish causal relationships between individual genes and specific phenotypes in patients with chromosomal deletion syndromes. Clinical manifestations of a monogenic disorder in a chromosomal deletion syndrome have also been reported for GATA3 haploinsufficiency (*64*). Our observations suggest that the study of rare IEIs can help to clarify phenotypes seen in individuals with more common chromosomal abnormalities.

In ORAS patients, autoinflammation results from the defective down-regulation of NF-κB-dependent inflammatory signaling in hematopoietic cells, particularly those of the myeloid lineage (*29–32*). OTULIN deficiency causes a gene dosage-dependent accumulation of M1-Ub, but OTULIN haploinsufficiency is both clinically and biochemically silent for TNF-induced signaling events, instead causing a predisposition to infection. The apparent paradox of autoinflammation and immunodeficiency within the spectrum of clinical phenotypes of OTULIN deficiency is also observed in patients with HOIL1 and HOIP deficiencies, which greatly decrease the levels of M1-Ub (*46, 65*). The combination of autoinflammation and immunodeficiency in HOIL1 and HOIP deficiencies highlights the complex role of LUBAC in maintaining the cell type-specific balance between inflammation and immunity. Inflammation is regulated by two other deubiquitinases in addition to OTULIN: A20 and CYLD. Phosphorylated A20 preferentially cleaves K63-Ub in cells (*66, 67*). CYLD hydrolyzes K63-Ub and M1-Ub (*68*). AD A20 deficiency causes an autoinflammatory condition resembling Behçet's disease (*69*), whereas AD CYLD deficiency results in cylindromatosis of the skin (*70*). AR HOIL1, HOIP, and OTULIN deficiencies and AD A20 deficiency are systemic disorders. Conversely,

AD OTULIN and CYLD deficiencies result in tissue-specific disease. OTULIN and CYLD bind HOIP in a mutually exclusive manner (*71*). The detection of CYLD bound to M1-Ub reveals another, LUBAC-independent, layer of crosstalk between the two deubiquitinases. CYLD activity and specificity were recently shown to be regulated by phosphorylation and ubiquitin-binding CAP-Gly domains (*72*). We speculate that, with insufficient amounts of OTULIN, phosphorylated CYLD primed for activity toward K63-Ub is quenched by M1-Ub. The accumulation of caveolin-1 in dermal fibroblasts observed in patients with OTULIN deficiency probably results from disruption of the polyubiquitination of this molecule.

Human OTULIN haploinsufficiency is an inborn error of cell-intrinsic immunity to *S. aureus* infection. Staphylococcal disease displays a remarkable organ tropism, affecting the skin and lungs in particular (*1*). Tissue barrier disruption is a hallmark of severe staphylococcal disease (*73*). α-Toxin is a key staphylococcal virulence factor that contributes to severe disease (*73–76*) and can injure non-hematopoietic cells (*54, 73, 77, 78*). The mechanism underlying the impairment of staphylococcal immunity in OTULIN haploinsufficiency is reminiscent of that involved in cell-intrinsic immunodeficiencies conferring susceptibility to viral infections (*79–81*). In the absence of sufficient levels of α-toxin-neutralizing antibodies, susceptibility to staphylococcal disease in patients with OTULIN haploinsufficiency is driven by a defect of cell-intrinsic immunity to the α-toxin of the pathogen. In patients with OTULIN haploinsufficiency, caveolin-1 accumulates specifically in non-hematopoietic cells. Caveolin-1 clusters with α-toxin and the retention of ADAM10 at the surface of the patients' cells predisposes these cells to α-toxin-induced cell death (*82, 83*). Caveolin-1 accumulation is observed in the cells of patients with either bi- or monoallelic OTULIN deficiencies. The late-onset infectious phenotype in patients with AD OTULIN deficiency may be overshadowed by the early-onset severe autoinflammatory manifestations in ORAS or compensated for by the presence of α-toxin-neutralizing antibodies. Consistent with this view, we also identified a pediatric homozygous carrier of a moderately hypomorphic OTULIN variant with an infectious phenotype indistinguishable from that of our haploinsufficient probands, with no autoinflammatory features. This work provides a direct demonstration of a defined host characteristic predisposing humans to adverse events elicited by a specific bacterial virulence factor.

S. aureus is a pathogen of paramount significance in human health (*1*). In the face of a globally emerging epidemic of community-acquired methicillin-resistant *S. aureus* (MRSA) strains (*18*), innovative strategies for treating and preventing infection are needed (*84*). In the presence or absence of documented *S. aureus* infections, OTULIN-haploinsufficient patients with severe necrosis may benefit from combined antibiotic and steroid therapy, together with α-toxin-neutralizing monoclonal antibodies (*85*). Despite clear public health needs, no effective *S. aureus* vaccine has yet been approved (*86*). Humans are the main reservoir of *S. aureus*, and the pathogen is highly adapted to its human host (*77, 78*). Mice are naturally resistant to *S. aureus* infection (*87*). The principal mechanistic differences in hematopoietic immunity to staphylococcal infections between humans and mice have been characterized (*77, 78*). By contrast, the mechanisms of cell-intrinsic immunity in non-hematopoietic cells have been little studied in either humans or mice (*80, 88–90*). Staphylococcal virulence factors, such as α-toxin, are considered potential targets for strategies aiming to treat and prevent infection (*77, 78*). For many of these virulence factors, and cytotoxins in particular, one or more aspects of the interaction with the host are human-specific (*78, 91*). Murine ADAM10 can interact with α-toxin (*55*). However, OTULIN haploinsufficiency reveals a layer of human specificity at the interface between α-toxin and its human non-hematopoietic target cells. OTULIN haploinsufficiency demonstrates the contribution of *S. aureus* toxins to the pathophysiology of severe disease in humans. The experiment of Nature described here identifies a mechanism of human cell-intrinsic immunity to *S. aureus* infections and highlights the potential for interfering with the staphylococcal α-toxin for treating and preventing disease (*85, 92*).

Materials and methods summary
Human subjects
Informed consent was obtained from each patient, in accordance with local regulations, and a protocol for research on human subjects was approved by the institutional review boards (IRB) of *Institut National de la Santé et de la Recherche Médicale* (INSERM, protocol C10-16) and The Rockefeller University (protocols JCA-0698 and JCA-0695).

Whole-exome sequencing, breakpoint determination, and variant enrichment analyses
Genomic DNA was extracted from whole blood. Whole-exome sequencing and breakpoint determinations are detailed in the SM. A gene-based enrichment analysis was performed on the cohort of 105 patients with severe staphylococcal disease, together with 1,274 individuals with Mendelian susceptibility to mycobacterial disease (MSMD) or suffering from tuberculosis (TB) as controls. Rare variants [MAF < 1×10^{-5} in the gnomAD database (*20*)] predicted to be damaging [combined annotation-dependent depletion score (CADD) > mutation significance cutoff (MSC) (*21*)] were retained (table S1) (*23*). The proportions of individuals with rare damaging variants in the cohort and the controls were compared by logistic regression with likelihood ratio tests (table S2). The first five principal components of the PCA were systematically

included in the logistic regression model to account for the ethnic heterogeneity of the cohorts, as previously described (*93*). Genes were then tested under a dominant genetic model. Four carriers, three of whom carried heterozygous variants, were identified amongst the cases. No carriers were identified amongst the controls. We then performed the same analysis again, but with the addition of 2,504 individuals from 1,000 Genomes Project phase 3 (*25*) to our control dataset (*26*).

Cell culture

Primary dermal fibroblasts (PDFs) were obtained from skin biopsy specimens and cultured in Dulbecco's modified Eagle's medium (DMEM) (Gibco) supplemented with 10% heat-inactivated fetal bovine serum (HI-FBS) (Gibco) unless otherwise specified. PBMCs were isolated from whole blood by density gradient centrifugation on Ficoll-Paque PLUS (GE Healthcare Life Sciences) and maintained in Roswell Park Memorial Institute (RPMI) 1640 (Gibco) medium supplemented with 10% HI-FBS unless otherwise specified. Immortalized fibroblasts were generated by transformation with SV40 as previously described (*94*) and maintained in DMEM supplemented with 10% HI-FBS. HEK293T cells (American Type Culture Collection) were cultured in DMEM supplemented with 10% HI-FBS.

Generation of OTULIN constructs, transfection, transduction, and nucleofection

The human canonical *OTULIN* cDNA open reading frame clone was amplified from pCMV6-Entry FAM105B (OriGene) and inserted into the pCMV6-AN-Myc-DDK-tagged vector (OriGene) or pLentiIII-UBC (Abmgood). Site-directed mutagenesis to generate the *OTULIN* variants present in the patients was performed by a modified overlap-extension PCR-based method (*95*). All constructs were validated by Sanger sequencing. HEK293T cells were transiently transfected in the presence of Lipofectamine LTX (Thermo Fisher Scientific). For lentiviral transductions, semi-confluent HEK293T cells were cotransfected with *OTULIN*, *GAG*, *POL*, and *ENV* plasmids. The supernatant was collected at 48 hours and 72 hours and concentrated with a Lenti-X concentrator (Clontech). A ten-fold dilution (by volume) of the lentivirus preparation was added to semi-confluent immortalized fibroblasts plated on six-well plates. Transduced cells were selected with puromycin (Invitrogen). PDFs were mixed with gene knockout kit V2 single guide RNA pools (Synthego) in the presence of TrueCut Cas9 protein V2 (Thermo Fisher Scientific), or with pCMV6 expression vectors, and nucleofected with the basic nucleofector kit for primary mammalian fibroblasts (Lonza) on a Nucleofector 2b device (Lonza).

NF-κB inhibition assay and linear deubiquitinase assay

HEK293T cells in 96-well plates were transiently cotransfected with pCMV6 vectors containing the *OTULIN* cDNA variants, the NF-κB firefly luciferase plasmid pGL4.32, and the *Renilla* luciferase plasmid (pRLTK) as an internal control. The cells were stimulated, 24 hours after transfection, by incubation with 20 ng/ml TNF in minimal medium (1% FBS) for an additional 24 hours. The ratio of firefly-to-*Renilla* luciferase expression was assessed with the Dual-Glo Luciferase assay (Promega) on a bioluminescence plate reader. Data were normalized against the inhibitory activity of cells transfected with a vector encoding the *OTULIN* reference cDNA. For linear deubiquitination assays, HEK293T cells were cotransfected with pCMV6 vectors containing the *OTULIN* cDNA variants, HOIL-1, HOIP, SHARPIN and linear ubiquitin (UbK0) and harvested after 48 hours. Whole-cell lysates (WCLs) were prepared with WCL buffer A (table S4). For immunoprecipitation, anti-M1-Ub antibody was added and the lysates were incubated overnight at room temperature. Dynabeads Protein G (Thermo Fisher Scientific) beads were added to the samples, which were then incubated for one hour at room temperature. The beads were then washed with WCL buffer A (table S4) and resuspended in 2 x NuPAGE LDS sample buffer (Thermo Fisher Scientific) supplemented with DTT. The antibodies used are described in table S3.

Reverse transcription and PCR

Total RNA was extracted from transiently transfected HEK293T cells or from PDFs with the RNeasy Mini Kit (QIAGEN). Reverse transcription was performed with the SuperScript III First-Strand Synthesis System (Invitrogen) and random hexamers. Quantitative PCR was performed with the TaqMan Universal PCR Master Mix (Applied Biosystems) in the 7500 Fast Real-Time PCR System (Applied Biosystems). The following TaqMan Gene Expression assays (Thermo Fisher Scientific) were used: *OTULIN* (Hs01113237_m1); *GUSB* (Hs00939627_m1); *GAPDH* (Hs99999905_m1).

Whole-cell lysates, SDS-PAGE, and Western blotting

Transiently transfected HEK293T cells were harvested and lysed in whole cell lysate (WCL) buffer B (table S4). PDFs were synchronized by incubation in DMEM containing 1% FBS for 24 hours before trypsin treatment and were then lysed in WCL buffer C (table S4) with sonication to clear the supernatants. Immortalized fibroblasts were stimulated with 10 ng/ml TNF and lysed in WCL buffer D (table S4). Monocytes were obtained from freshly thawed PBMCs with the Pan Monocyte Isolation Kit (Miltenyi Biotec) and lysed in WCL buffer C (table S4) with sonication to clear the supernatants. Laemmli buffer (BioRad) supplemented with DTT was added to the clarified lysates. Proteins were separated by SDS–PAGE

transferred onto an Immobilon-P PVDF membrane (Millipore). The membrane was blocked by incubation in PBS supplemented with 0.1% Tween 20 and 5% BSA and incubated overnight with the primary antibody, followed by the appropriate horseradish peroxidase-conjugated secondary antibody. Immunoreactive proteins were visualized by enhanced chemiluminescence. Intensity analyses were performed with ImageStudioLite (LI-COR). The antibodies used are described in table S3.

Cytometry by time-of-flight

Freshly thawed PBMCs were incubated with Fc block and then with a panel of metal-conjugated antibodies, as described elsewhere (96). The antibodies used are described in table S3. Batch-integrated unsupervised clustering analysis was conducted with the iMUBAC pipeline (45). The analysis included 29 adult controls (nine studied in replicate) and nine pediatric controls (all under the age of 18 years) studied across seven batches of experiments, four patients with heterozygous mutations of *OTULIN* and two 5p- patients studied in two batches of experiments. Clusters were identified manually and renamed based on their marker expression patterns.

Flow cytometry

Freshly thawed PBMCs were rested for 3 hours and were then stimulated for 90 min with 20 ng/ml TNF (R&D Systems) or 1 ng/ml LPS (InvivoGen). The reaction was stopped by washing the cells with PBS, and the cells were then subjected to live/dead staining. Cells were subsequently stained with surface markers and washed. They were then permeabilized and stained with Phosflow Perm Buffer (BD) or Intracellular Staining Perm Wash Buffer (BioLegend). PDFs were synchronized by incubation in DMEM supplemented with 1% HI-FBS for 24 hours and were then harvested by trypsin treatment. The fibroblasts were stained, fixed and acquired on a LSR-Fortessa cytometer (BD). All flow cytometry results were analyzed with FlowJo (version 10). The antibodies used are described in table S3.

Cytokine detection

PDFs were synchronized by incubation in DMEM supplemented with 1% HI-FBS for 24 hours before stimulation. At steady state and after 6 hours of stimulation with 20 ng/ml TNF (R&D Systems), supernatants were harvested, and the levels of IL-6 and IL-8 were assessed with the IL-6 and IL-8 Human ELISA kits (Thermo Fisher Scientific). Freshly thawed PBMCs were left unstimulated or stimulated with 20 ng/ml TNF (R&D Systems), 10 ng/ml IL-1β (R&D Systems), HKSA (heat-killed *S. aureus*; MOI: 10; InvivoGen), or 1 ng/ml LPS (InvivoGen) for 6 hours. Supernatants were harvested, and chemokines and cytokines were detected with

LEGENDPlex Human Inflammation Panel 1 (BioLegend).

Induced pluripotent stem cells

The generation and culture of iPSCs, their differentiation into macrophages, and the phagocytosis and H_2O_2 production assays are described in the SM.

Transcriptional and proteomic analyses

Transcriptional analyses in PDFs and PBMCs, single-cell RNA-sequencing on PBMCs, and global proteomics analyses of PDFs are described in the SM.

Caveolin-1 immune purification from whole-cell lysates

PDFs were synchronized by incubation in DMEM containing 1% HI-FBS for 24 hours and were then harvested by trypsin treatment. Cell pellets were lysed in WCL buffer C (table S4) with sonication to clear the supernatants. Cleared WCLs were incubated overnight at 4°C with Protein A Dynabeads (Thermo Fisher Scientific) conjugated to the monoclonal anti-caveolin-1 antibody or an isotype control. The samples were then eluted from the beads with 50 mM glycine, pH 2. The antibodies used are described in table S3. The immuno-purification products (IPs) were then split into portions for loading onto a gel or direct in-solution proteomic analyses, as described in the SM.

Deubiquitination of purified caveolin-1

Caveolin-1 IPs were treated with recombinant deubiquitinases as described elsewhere (97). Briefly, immunopurified caveolin-1 was incubated with deubiquitinases at 37°C for 30 min. Recombinant USP2, AMSH, and OTULIN (UbiCREST Deubiquitinase Enzyme Set, R&D Systems) were used at a final concentration of 1x. Recombinant His-CYLD (R&D Systems) was used at a final concentration of 1 μM. Purified polyubiquitin chains were deubiquitinated by incubating tetra-M1-, K48- and K63-Ub chains (R&D Systems) at a concentration of 3 μM with deubiquitinases. Following the enzymatic reactions, sample buffer containing DTT was added, and the proteins were separated by SDS-PAGE, as described above.

Linear ubiquitin-selective tandem Ub-binding entity assay

For M1-Ub pulldown, immortalized fibroblasts were lysed in WCL buffer E (table S4) containing FLAG-tagged M1-Ub-selective tandem Ub-binding entity (TUBE) (LifeSensors). Supernatants were cleared by centrifugation and incubated with Anti-FLAG M2 agarose beads (Sigma Aldrich) for 2 hours at 4°C. The beads were washed with WCL buffer E (table S4), and resuspended in 1 x Laemmli buffer without reducing agent. For M1-Ub quantification, we used an input of ~0.5 mg per sample. For the identification of peptides bound

to M1-Ub, we used an input of ~2 mg per sample. M1-Ub quantification and the identification of peptides bound to M1-Ub by means of absolute quantification (AQUA) tandem mass spectrometry (MS/MS) are described in the SM. For western-blot analyses, beads were resuspended in sample buffer containing DTT and samples were separated by SDS-PAGE, as described above.

Immunofluorescence assays

Immortalized fibroblasts were cultured on glass coverslips for the staining of M1-Ub, K63-Ub, and caveolin-1. The cells were fixed in methanol, blocked by incubation with 1% BSA and incubated overnight with primary antibodies and Cell-Mask deep red plasma membrane stain (Thermo Fisher Scientific), followed by secondary antibodies and DAPI. Specimens were examined either with an Imager Z1 microscope (Carl Zeiss, for M1-Ub aggregate number quantifications) or a LSM800 laser scanning microscope (Carl Zeiss, for caveolin-1 and M1-Ub or K63-Ub colocalization experiments). The numbers of ubiquitin aggregates per cell were quantified using CellProfiler (http://www.cellprofiler.org/). Nuclei and cell boundaries were segmented to identify OTULIN-positive cells and to attribute M1-Ub-positive aggregates to parental cells. Immunofluorescence deubiquitination and competition assays are described in the SM. For α-toxin colocalization and binding experiments, PDFs were synchronized by incubation in DMEM containing 1% HI-FBS for 24 hours before trypsin treatment. PDFs were incubated with 10 μg/ml α-toxin-Cys-AF647, washed, and then fixed with methanol. After incubation with antibodies and DAPI, cells were seeded in a slide chamber. Images were acquired on a Leica SP5 confocal microscope (Leica Microsystems) and NanoImager (ONI). In parallel, the cells were recorded on a FACS Verse flow cytometer (BD). Confocal images were analyzed with Image J Fiji software and the JACoP colocalization analysis plugin (98). The antibodies used are described in table S3.

Cell viability assays

PDFs were plated in a microtiter plate and synchronized in DMEM containing 1% HI-FBS and 25 mM DMEM for 24 hours and were then incubated for 2.5 hours with 5-10% crude bacterial culture supernatant or for 24 hours with recombinant toxins, or with 100 ng/ml TNF (R&D Systems) plus 1 μM BV6 (ApexBio) at 37°C, under an atmosphere containing 5% CO_2. Bacterial supernatants were neutralized by incubation for 15 min in DMEM supplemented with 10% HI-FBS plus 100 μg/ml monoclonal antibodies (92, 99). PBMCs and iPSC-derived macrophages were incubated with α-toxin for 2 hours and 24 hours, respectively, at 37°C, under an atmosphere containing 5% CO_2. For the inhibition of α-toxin cytotoxicity, PDFs were treated for 1 hour with 20 μM GI-254023X (R&D Systems) or DMSO before adding 1.1 μg/ml α-

toxin, or for 2 hours with 1 mM methyl-β-cyclodextrin (Sigma) followed by washing and the addition of 1.1 μg/ml α-toxin. Viability was assessed with the CellTiterGlo Luminescent Cell Viability Assay (Promega) and expressed relative to cells not incubated with the toxin or supernatant. Four-parameter non-linear regression analyses were performed to obtain half-maximum effective concentrations (EC_{50}). The expression of recombinant toxins and the generation of bacterial culture supernatant are described in the SM.

Metalloprotease activity assays

PDFs were plated in a microtiter plate and synchronized by incubation in DMEM containing 1% HI-FBS and 25 mM DMEM for 24 hours. They were then treated for 1 hour with 20 μM GI-254023X (R&D Systems) or DMSO before the addition of 3.3 μg/ml wild-type or H35L-toxoid α-toxin. After 2 hours of incubation at 37°C, under an atmosphere containing 5% CO_2, cells were washed with 25 mM Tris (pH 8), and 10 μM Mca-PLAQAV-Dpa-RSSSR-NH2 Fluorogenic Peptide Substrate (R&D Systems) was added. After incubation for 30 min, fluorescence intensity was measured on a monochromator-based microplate reader and expressed relative to cells not incubated with the toxin.

Mice

The generation and use of *Otulin*-haploinsufficient mice is described in the SM.

Anti-α-toxin immunoglobulins

The capacity of the plasma to neutralize microbial toxins was assessed with rabbit erythrocytes, as described in the SM. Pooled plasma was depleted of IgG with HiTrap Protein G HRP columns (GE Healthcare). Anti-α-toxin immunoglobulin levels were measured by ELISA, as described in the SM.

REFERENCES AND NOTES

1. F. D. Lowy, *Staphylococcus aureus* infections. *N. Engl. J. Med.* **339**, 520–532 (1998). doi:10.1056/NEJM199808203390806 Medline
2. Y. Gillet, B. Issartel, P. Vanhems, J.-C. Fournet, G. Lina, M. Bes, F. Vandenesch, Y. Piémont, N. Brousse, D. Floret, J. Etienne, Association *between Staphylococcus aureus* strains carrying gene for Panton-Valentine leukocidin and highly lethal necrotising pneumonia in young immunocompetent patients. *Lancet* **359**, 753–759 (2002). doi:10.1016/S0140-6736(02)07877-7 Medline
3. A. I. Hidron, C. E. Low, E. G. Honig, H. M. Blumberg, Emergence of community-acquired meticillin-resistant *Staphylococcus aureus* strain USA300 as a cause of necrotising community-onset pneumonia. *Lancet Infect. Dis.* **9**, 384–392 (2009). doi:10.1016/S1473-3099(09)70133-1 Medline
4. G. Lina, Y. Piémont, F. Godail-Gamot, M. Bes, M.-O. Peter, V. Gauduchon, F. Vandenesch, J. Etienne, Involvement of Panton-Valentine leukocidin-producing *Staphylococcus aureus* in primary skin infections and pneumonia. *Clin. Infect. Dis.* **29**, 1128–1132 (1999). doi:10.1086/313461 Medline
5. F. Vandenesch, T. Naimi, M. C. Enright, G. Lina, G. R. Nimmo, H. Heffernan, N. Liassine, M. Bes, T. Greenland, M.-E. Reverdy, J. Etienne, Community-acquired methicillin-resistant *Staphylococcus aureus* carrying Panton-Valentine leukocidin genes: Worldwide emergence. *Emerg. Infect. Dis.* **9**, 978–984 (2003). doi:10.3201/eid0908.030089 Medline

6. B. Boisson, The genetic basis of pneumococcal and staphylococcal infections: Inborn errors of human TLR and IL-1R immunity. *Hum. Genet.* **139**, 981–991 (2020). doi:10.1007/s00439-020-02111-z Medline

7. S. G. Tangye, W. Al-Herz, A. Bousfiha, C. Cunningham-Rundles, J. L. Franco, S. M. Holland, C. Klein, T. Morio, E. Oksenhendler, C. Picard, A. Puel, J. Puck, M. R. J. Seppänen, R. Somech, H. C. Su, K. E. Sullivan, T. R. Torgerson, I. Meyts, The ever-increasing array of novel inborn errors of immunity: An interim update by the IUIS Committee. *J. Clin. Immunol.* **41**, 666–679 (2021). doi:10.1007/s10875-021-00980-1 Medline

8. C. Picard, A. Puel, M. Bonnet, C.-L. Ku, J. Bustamante, K. Yang, C. Soudais, S. Dupuis, J. Feinberg, C. Fieschi, C. Elbim, R. Hitchcock, D. Lammas, G. Davies, A. Al-Ghonaium, H. Al-Rayes, S. Al-Jumaah, S. Al-Hajjar, I. Z. Al-Mohsen, H. H. Frayha, R. Rucker, T. R. Hawn, A. Aderem, H. Tufenkeji, S. Haraguchi, N. K. Day, R. A. Good, M.-A. Gougerot-Pocidalo, A. Ozinsky, J.-L. Casanova, Pyogenic bacterial infections in humans with IRAK-4 deficiency. *Science* **299**, 2076–2079 (2003). doi:10.1126/science.1081902 Medline

9. C. Picard, H. von Bernuth, P. Ghandil, M. Chrabieh, O. Levy, P. D. Arkwright, D. McDonald, R. S. Geha, H. Takada, J. C. Krause, C. B. Creech, C.-L. Ku, S. Ehl, L. Maródi, S. Al-Muhsen, S. Al-Hajjar, A. Al-Ghonaium, N. K. Day-Good, S. M. Holland, J. I. Gallin, H. Chapel, D. P. Speert, C. Rodriguez-Gallego, E. Colino, B.-Z. Garty, C. Roifman, T. Hara, H. Yoshikawa, S. Nonoyama, J. Domachowske, A. C. Issekutz, M. Tang, J. Smart, S. E. Zitnik, C. Hoarau, D. S. Kumararatne, A. J. Thrasher, E. G. Davies, C. Bethune, N. Sirvent, D. de Ricaud, Y. Camcioglu, J. Vasconcelos, M. Guedes, A. B. Vitor, C. Rodrigo, F. Almazán, M. Méndez, J. I. Aróstegui, L. Alsina, C. Fortuny, J. Reichenbach, J. W. Verbsky, X. Bossuyt, R. Doffinger, L. Abel, A. Puel, J.-L. Casanova, Clinical features and outcome of patients with IRAK-4 and MyD88 deficiency. *Medicine* **89**, 403–425 (2010). doi:10.1097/MD.0b013e3181fd8ec3 Medline

10. C. Picard, J. L. Casanova, A. Puel, Infectious diseases in patients with IRAK-4, MyD88, NEMO, or IκBα deficiency. *Clin. Microbiol. Rev.* **24**, 490–497 (2011). doi:10.1128/CMR.00001-11 Medline

11. H. von Bernuth, C. Picard, Z. Jin, R. Pankla, H. Xiao, C.-L. Ku, M. Chrabieh, I. B. Mustapha, P. Ghandil, Y. Camcioglu, J. Vasconcelos, N. Sirvent, M. Guedes, A. B. Vitor, M. J. Herrero-Mata, J. I. Aróstegui, C. Rodrigo, L. Alsina, E. Ruiz-Ortiz, M. Juan, C. Fortuny, J. Yagüe, J. Antón, M. Pascal, H.-H. Chang, L. Janniere, Y. Rose, B.-Z. Garty, H. Chapel, A. Issekutz, L. Maródi, C. Rodriguez-Gallego, J. Banchereau, L. Abel, X. Li, D. Chaussabel, A. Puel, J.-L. Casanova, Pyogenic bacterial infections in humans with MyD88 deficiency. *Science* **321**, 691–696 (2008). doi:10.1126/science.1158298 Medline

12. L. Israel, Y. Wang, K. Bulek, E. Della Mina, Z. Zhang, V. Pedergnana, M. Chrabieh, N. A. Lemmens, V. Sancho-Shimizu, M. Descatoire, T. Lasseau, E. Israelsson, L. Lorenzo, L. Yun, A. Belkadi, A. Moran, L. E. Weisman, F. Vandenesch, F. Batteux, S. Weller, M. Levin, J. Herberg, A. Abhyankar, C. Prando, Y. Itan, W. J. B. van Wamel, C. Picard, L. Abel, D. Chaussabel, X. Li, B. Beutler, P. D. Arkwright, J.-L. Casanova, A. Puel, Human adaptive immunity rescues an inborn error of innate immunity. *Cell* **168**, 789–800.e10 (2017). doi:10.1016/j.cell.2017.01.039 Medline

13. A. Puel, C. Picard, M. Lorrot, C. Pons, M. Chrabieh, L. Lorenzo, M. Mamani-Matsuda, E. Jouanguy, D. Gendrel, J.-L. Casanova, Recurrent staphylococcal cellulitis and subcutaneous abscesses in a child with autoantibodies against IL-6. *J. Immunol.* **180**, 647–654 (2008). doi:10.4049/jimmunol.180.1.647 Medline

14. T. Schwerd, S. R. F. Twigg, D. Aschenbrenner, S. Manrique, K. A. Miller, I. B. Taylor, M. Capitani, S. J. McGowan, E. Sweeney, A. Weber, L. Chen, P. Bowness, A. Riordan, A. Cant, A. F. Freeman, J. D. Milner, S. M. Holland, N. Frede, M. Müller, D. Schmidt-Arras, B. Grimbacher, S. A. Wall, E. Y. Jones, A. O. M. Wilkie, H. H. Uhlig, A biallelic mutation in *IL6ST* encoding the GP130 co-receptor causes immunodeficiency and craniosynostosis. *J. Exp. Med.* **214**, 2547–2562 (2017). doi:10.1084/jem.20161810 Medline

15. V. Béziat, J. Li, J.-X. Lin, C. S. Ma, P. Li, A. Bousfiha, I. Pellier, S. Zoghi, S. Baris, S. Keles, P. Gray, N. Du, Y. Wang, Y. Zerbib, R. Lévy, T. Leclercq, F. About, A. I. Lim, G. Rao, K. Payne, S. J. Pelham, D. T. Avery, E. K. Deenick, B. Pillay, J. Chou, R. Guery, A. Belkadi, A. Guérin, M. Migaud, V. Rattina, F. Ailal, I. Benhsaien, M. Bouaziz, T. Habib, D. Chaussabel, N. Marr, J. El-Benna, B. Grimbacher, O. Wargon, J. Bustamante, B. Boisson, I. Müller-Fleckenstein, B. Fleckenstein, M.-O. Chandesris, M. Titeux, S. Fraitag, M.-A. Alyanakian, M. Leruez-Ville, C. Picard, I. Meyts, J. P. Di Santo, A. Hovnanian, A. Somer, A. Ozen, N. Rezaei, T. A. Chatila, L.

Abel, W. J. Leonard, S. G. Tangye, A. Puel, J.-L. Casanova, A recessive form of hyper-IgE syndrome by disruption of ZNF341-dependent STAT3 transcription and activity. *Sci. Immunol.* **3**, eaat4956 (2018). doi:10.1126/sciimmunol.aat4956 Medline

16. Y. Minegishi, M. Saito, S. Tsuchiya, I. Tsuge, H. Takada, T. Hara, N. Kawamura, T. Ariga, S. Pasic, O. Stojkovic, A. Metin, H. Karasuyama, Dominant-negative mutations in the DNA-binding domain of STAT3 cause hyper-IgE syndrome. *Nature* **448**, 1058–1062 (2007). doi:10.1038/nature06096 Medline

17. S. Spencer, S. Köstel Bal, W. Egner, H. Lango Allen, S. I. Raza, C. A. Ma, M. Gürel, Y. Zhang, G. Sun, R. A. Sabroe, D. Greene, W. Rae, T. Shahin, K. Kania, R. C. Ardy, M. Thian, E. Staples, A. Pecchia-Bekkum, W. P. M. Worrall, J. Stephens, M. Brown, S. Tuna, M. York, F. Shackley, D. Kerrin, R. Sargur, A. Condliffe, H. N. Tipu, H. S. Kuehn, S. D. Rosenzweig, E. Turro, S. Tavaré, A. J. Thrasher, D. I. Jodrell, K. G. C. Smith, K. Boztug, J. D. Milner, J. E. D. Thaventhiran, Loss of the interleukin-6 receptor causes immunodeficiency, atopy, and abnormal inflammatory responses. *J. Exp. Med.* **216**, 1986–1998 (2019). doi:10.1084/jem.20190344 Medline

18. F. R. DeLeo, M. Otto, B. N. Kreiswirth, H. F. Chambers, Community-associated meticillin-resistant *Staphylococcus aureus*. *Lancet* **375**, 1557–1568 (2010). doi:10.1016/S0140-6736(09)61999-1 Medline

19. L. J. Shallcross, E. Fragaszy, A. M. Johnson, A. C. Hayward, The role of the Panton-Valentine leucocidin toxin in staphylococcal disease: A systematic review and meta-analysis. *Lancet Infect. Dis.* **13**, 43–54 (2013). doi:10.1016/S1473-3099(12)70238-4 Medline

20. K. J. Karczewski, L. C. Francioli, G. Tiao, B. B. Cummings, J. Alföldi, Q. Wang, R. L. Collins, K. M. Laricchia, A. Ganna, D. P. Birnbaum, L. D. Gauthier, H. Brand, M. Solomonson, N. A. Watts, D. Rhodes, M. Singer-Berk, E. M. England, E. G. Seaby, J. A. Kosmicki, R. K. Walters, K. Tashman, Y. Farjoun, E. Banks, T. Poterba, A. Wang, C. Seed, N. Whiffin, J. X. Chong, K. E. Samocha, E. Pierce-Hoffman, Z. Zappala, A. H. O'Donnell-Luria, E. V. Minikel, B. Weisburd, M. Lek, J. S. Ware, C. Vittal, I. M. Armean, L. Bergelson, K. Cibulskis, K. M. Connolly, M. Covarrubias, S. Donnelly, S. Ferriera, S. Gabriel, J. Gentry, N. Gupta, T. Jeandet, D. Kaplan, C. Llanwarne, R. Munshi, S. Novod, N. Petrillo, D. Roazen, V. Ruano-Rubio, A. Saltzman, M. Schleicher, J. Soto, K. Tibbetts, C. Tolonen, G. Wade, M. E. Talkowski, B. M. Neale, M. J. Daly, D. G. MacArthur; Genome Aggregation Database Consortium, The mutational constraint spectrum quantified from variation in 141,456 humans. *Nature* **581**, 434–443 (2020). doi:10.1038/s41586-020-2308-7 Medline

21. Y. Itan, L. Shang, B. Boisson, M. J. Ciancanelli, J. G. Markle, R. Martinez-Barricarte, E. Scott, I. Shah, P. D. Stenson, J. Gleeson, D. N. Cooper, L. Quintana-Murci, S.-Y. Zhang, L. Abel, J.-L. Casanova, The mutation significance cutoff: Gene-level thresholds for variant predictions. *Nat. Methods* **13**, 109–110 (2016). doi:10.1038/nmeth.3739 Medline

22. M. Kircher, D. M. Witten, P. Jain, B. J. O'Roak, G. M. Cooper, J. Shendure, A general framework for estimating the relative pathogenicity of human genetic variants. *Nat. Genet.* **46**, 310–315 (2014). doi:10.1038/ng.2892 Medline

23. P. Zhang, B. Bigio, F. Rapaport, S.-Y. Zhang, J.-L. Casanova, L. Abel, B. Boisson, Y. Itan, PopViz: A webserver for visualizing minor allele frequencies and damage prediction scores of human genetic variations. *Bioinformatics* **34**, 4307–4309 (2018). doi:10.1093/bioinformatics/bty536 Medline

24. L. D. Notarangelo, R. Bacchetta, J. L. Casanova, H. C. Su, Human inborn errors of immunity: An expanding universe. *Sci. Immunol.* **5**, eabb1662 (2020). doi:10.1126/sciimmunol.abb1662 Medline

25. 1000 Genomes Project Consortium, A global reference for human genetic variation. *Nature* **526**, 68–74 (2015). doi:10.1038/nature15393 Medline

26. S. Boisson-Dupuis, N. Ramirez-Alejo, Z. Li, E. Patin, G. Rao, G. Kerner, C. K. Lim, D. N. Krementsov, N. Hernandez, C. S. Ma, Q. Zhang, J. Markle, R. Martinez-Barricarte, K. Payne, R. Fisch, C. Deswarte, J. Halpern, M. Bouaziz, J. Mulwa, D. Sivanesan, T. Lazarov, R. Naves, P. Garcia, Y. Itan, B. Boisson, A. Checchi, F. Jabot-Hanin, A. Cobat, A. Guennoun, C. C. Jackson, S. Pekcan, Z. Caliskaner, J. Inostroza, B. T. Costa-Carvalho, J. A. T. de Albuquerque, H. Garcia-Ortiz, L. Orozco, T. Ozcelik, A. Abid, I. A. Rhorfi, H. Souhi, H. N. Amrani, A. Zegmout, F. Geissmann, S. W. Michnick, I. Muller-Fleckenstein, B. Fleckenstein, A. Puel, M. J. Ciancanelli, N. Marr, H. Abolhassani, M. E. Balcells, A. Condino-Neto, A. Strickler, K. Abarca, C. Teuscher, H. D. Ochs, I. Reisli, E. H. Sayar, J. El-Baghdadi, J.

Bustamante, L. Hammarström, S. G. Tangye, S. Pellegrini, L. Quintana-Murci, L. Abel, J.-L. Casanova, Tuberculosis and impaired IL-23–dependent IFN-γ immunity in humans homozygous for a common *TYK2* missense variant. *Sci. Immunol.* **3**, eaau8714 (2018). doi:10.1126/sciimmunol.aau8714 Medline

27. K. Keusekotten, P. R. Elliott, L. Glockner, B. K. Fiil, R. B. Damgaard, Y. Kulathu, T. Wauer, M. K. Hospenthal, M. Gyrd-Hansen, D. Krappmann, K. Hofmann, D. Komander, OTULIN antagonizes LUBAC signaling by specifically hydrolyzing Met1-linked polyubiquitin. *Cell* **153**, 1312–1326 (2013). doi:10.1016/j.cell.2013.05.014 Medline

28. E. Rivkin, S. M. Almeida, D. F. Ceccarelli, Y.-C. Juang, T. A. MacLean, T. Srikumar, H. Huang, W. H. Dunham, R. Fukumura, G. Xie, Y. Gondo, B. Raught, A.-C. Gingras, F. Sicheri, S. P. Cordes, The linear ubiquitin-specific deubiquitinase gumby regulates angiogenesis. *Nature* **498**, 318–324 (2013). doi:10.1038/nature12296 Medline

29. R. B. Damgaard, P. R. Elliott, K. N. Swatek, E. R. Maher, P. Stepensky, O. Elpeleg, D. Komander, Y. Berkun, OTULIN deficiency in ORAS causes cell type-specific LUBAC degradation, dysregulated TNF signalling and cell death. *EMBO Mol. Med.* **11**, e9324 (2019). doi:10.15252/emmm.201809324 Medline

30. R. B. Damgaard, J. A. Walker, P. Marco-Casanova, N. V. Morgan, H. L. Titheradge, P. R. Elliott, D. McHale, E. R. Maher, A. N. J. McKenzie, D. Komander, The deubiquitinase OTULIN is an essential negative regulator of inflammation and autoimmunity. *Cell* **166**, 1215–1230.e20 (2016). doi:10.1016/j.cell.2016.07.019 Medline

31. M. Nabavi, M. Shahrooei, H. Rokni-Zadeh, J. Vrancken, M. Changi-Ashtiani, K. Darabi, M. Manian, F. Seif, I. Meyts, A. Voet, L. Moens, X. Bossuyt, Auto-inflammation in a patient with a novel homozygous OTULIN mutation. *J. Clin. Immunol.* **39**, 138–141 (2019). doi:10.1007/s10875-019-00599-3 Medline

32. Q. Zhou, X. Yu, E. Demirkaya, N. Deuitch, D. Stone, W. L. Tsai, H. S. Kuehn, H. Wang, D. Yang, Y. H. Park, A. K. Ombrello, M. Blake, T. Romeo, E. F. Remmers, J. J. Chae, J. C. Mullikin, F. Güzel, J. D. Milner, M. Boehm, S. D. Rosenzweig, M. Gadina, S. B. Welch, S. Özen, R. Topaloglu, M. Abinun, D. L. Kastner, I. Aksentijevich, Biallelic hypomorphic mutations in a linear deubiquitinase define otulipenia, an early-onset autoinflammatory disease. *Proc. Natl. Acad. Sci. U.S.A.* **113**, 10127–10132 (2016). doi:10.1073/pnas.1612594113 Medline

33. J. Zinngrebe, B. Moepps, T. Monecke, P. Gierschik, F. Schlichtig, T. F. E. Barth, G. Strauß, E. Boldrin, C. Posovszky, A. Schulz, O. Beringer, E. Rieser, E.-M. Jacobsen, M. R. Lorenz, K. Schwarz, U. Pannicke, H. Walczak, D. Niessing, C. Schuetz, P. Fischer-Posovszky, K.-M. Debatin, Compound heterozygous variants in OTULIN are associated with fulminant atypical late-onset ORAS. *EMBO Mol. Med.* **14**, e14901 (2022). doi:10.15252/emmm.202114901 Medline

34. A. Bousfiha, L. Jeddane, C. Picard, W. Al-Herz, F. Ailal, T. Chatila, C. Cunningham-Rundles, A. Etzioni, J. L. Franco, S. M. Holland, C. Klein, T. Morio, H. D. Ochs, E. Oksenhendler, J. Puck, T. R. Torgerson, J.-L. Casanova, K. E. Sullivan, S. G. Tangye, Human inborn errors of immunity: 2019 update of the IUIS phenotypical classification. *J. Clin. Immunol.* **40**, 66–81 (2020). doi:10.1007/s10875-020-00758-x Medline

35. K. E. Eilertson, J. G. Booth, C. D. Bustamante, SnIPRE: Selection inference using a Poisson random effects model. *PLOS Comput. Biol.* **8**, e1002806 (2012). doi:10.1371/journal.pcbi.1002806 Medline

36. F. Rapaport, B. Boisson, A. Gregor, V. Béziat, S. Boisson-Dupuis, J. Bustamante, E. Jouanguy, A. Puel, J. Rosain, Q. Zhang, S.-Y. Zhang, J. G. Gleeson, L. Quintana-Murci, J.-L. Casanova, L. Abel, E. Patin, Negative selection on human genes underlying inborn errors depends on disease outcome and both the mode and mechanism of inheritance. *Proc. Natl. Acad. Sci. U.S.A.* **118**, e2001248118 (2021). doi:10.1073/pnas.2001248118 Medline

37. J. Fadista, N. Oskolkov, O. Hansson, L. Groop, LoFtool: A gene intolerance score based on loss-of-function variants in 60 706 individuals. *Bioinformatics* **33**, 471–474 (2017). Medline

38. X. Zhang, A. Snijders, R. Segraves, X. Zhang, A. Niebuhr, D. Albertson, H. Yang, J. Gray, E. Niebuhr, L. Bolund, D. Pinkel, High-resolution mapping of genotype-phenotype relationships in cri du chat syndrome using array comparative genomic hybridization. *Am. J. Hum. Genet.* **76**, 312–326 (2005). doi:10.1086/427762 Medline

39. J. Lejeune, J. Lafourcade, R. Berger, J. Vialatte, M. Boeswillwald, P. Seringe, R. Turpin, Trois cas de d'el'etion partielle du bras court d'un chromosome 5 [3 cases

of partial deletion of the short arm of a 5 chromosome]. *C. R. Hebd. Seances Acad. Sci.* **257**, 3098–3102 (1963). Medline

40. E. Niebuhr, The Cri du chat syndrome: Epidemiology, cytogenetics, and clinical features. *Hum. Genet.* **44**, 227–275 (1978). doi:10.1007/BF00394291 Medline

41. P. Cerruti Mainardi, Cri du Chat syndrome. *Orphanet J. Rare Dis.* **1**, 33 (2006). doi:10.1186/1750-1172-1-33 Medline

42. P. C. Mainardi, G. Pastore, C. Castronovo, M. Godi, A. Guala, S. Tamiazzo, S. Provera, M. Pierluigi, F. D. Bricarelli, The natural history of Cri du Chat Syndrome. A report from the Italian Register. *Eur. J. Med. Genet.* **49**, 363–383 (2006). doi:10.1016/j.ejmg.2005.12.004 Medline

43. R. Seger, A. Wildfeuer, G. Buchinger, W. Romen, D. Catty, L. Dybas, O. Haferkamp, J. Ströder, Defects in granulocyte function in various chromosome abnormalities (Down's-, Edwards'-, Cri-du-chat syndrome). *Klin. Wochenschr.* **54**, 177–183 (1976). doi:10.1007/BF01468883 Medline

44. L. E. Wilkins, J. A. Brown, W. E. Nance, B. Wolf, Clinical heterogeneity in 80 home-reared children with cri du chat syndrome. *J. Pediatr.* **102**, 528–533 (1983). doi:10.1016/S0022-3476(83)80179-6 Medline

45. M. Ogishi, R. Yang, C. Gruber, P. Zhang, S. J. Pelham, A. N. Spaan, J. Rosain, M. Chbihi, J. E. Han, V. K. Rao, L. Kainulainen, J. Bustamante, B. Boisson, D. Bogunovic, S. Boisson-Dupuis, J.-L. Casanova, Multibatch cytometry data integration for optimal immunophenotyping. *J. Immunol.* **206**, 206–213 (2021). doi:10.4049/jimmunol.2000854 Medline

46. B. Boisson, E. Laplantine, C. Prando, S. Giliani, E. Israelsson, Z. Xu, A. Abhyankar, L. Israël, G. Trevejo-Nunez, D. Bogunovic, A.-M. Cepika, D. MacDuff, M. Chrabieh, M. Hubeau, F. Bajolle, M. Debré, E. Mazzolari, D. Vairo, F. Agou, H. W. Virgin, X. Bossuyt, C. Rambaud, F. Facchetti, D. Bonnet, P. Quartier, J.-C. Fournet, V. Pascual, D. Chaussabel, L. D. Notarangelo, A. Puel, A. Israël, J.-L. Casanova, C. Picard, Immunodeficiency, autoinflammation and amylopectinosis in humans with inherited HOIL-1 and LUBAC deficiency. *Nat. Immunol.* **13**, 1178–1186 (2012). doi:10.1038/ni.2457 Medline

47. A. Subramanian, P. Tamayo, V. K. Mootha, S. Mukherjee, B. L. Ebert, M. A. Gillette, A. Paulovich, S. L. Pomeroy, T. R. Golub, E. S. Lander, J. P. Mesirov, Gene set enrichment analysis: A knowledge-based approach for interpreting genome-wide expression profiles. *Proc. Natl. Acad. Sci. U.S.A.* **102**, 15545–15550 (2005). doi:10.1073/pnas.0506580102 Medline

48. A. Hayer, M. Stoeber, D. Ritz, S. Engel, H. H. Meyer, A. Helenius, Caveolin-1 is ubiquitinated and targeted to intralumenal vesicles in endolysosomes for degradation. *J. Cell Biol.* **191**, 615–629 (2010). doi:10.1083/jcb.201003086 Medline

49. M. Sato, R. Konuma, K. Sato, K. Tomura, K. Sato, Fertilization-induced K63-linked ubiquitylation mediates clearance of maternal membrane proteins. *Development* **141**, 1324–1331 (2014). doi:10.1242/dev.103044 Medline

50. M. Uhlén, L. Fagerberg, B. M. Hallström, C. Lindskog, P. Oksvold, A. Mardinoglu, Å. Sivertsson, C. Kampf, E. Sjöstedt, A. Asplund, I. Olsson, K. Edlund, E. Lundberg, S. Navani, C. A.-K. Szigyarto, J. Odeberg, D. Djureinovic, J. O. Takanen, S. Hober, T. Alm, P.-H. Edqvist, H. Berling, H. Tegel, J. Mulder, J. Rockberg, P. Nilsson, J. M. Schwenk, M. Hamsten, K. von Feilitzen, M. Forsberg, L. Persson, F. Johansson, M. Zwahlen, G. von Heijne, J. Nielsen, F. Pontén, Tissue-based map of the human proteome. *Science* **347**, 1260419 (2015). doi:10.1126/science.1260419 Medline

51. P. J. Thul, L. Åkesson, M. Wiking, D. Mahdessian, A. Geladaki, H. Ait Blal, T. Alm, A. Asplund, L. Björk, L. M. Breckels, A. Bäckström, F. Danielsson, L. Fagerberg, J. Fall, L. Gatto, C. Gnann, S. Hober, M. Hjelmare, F. Johansson, S. Lee, C. Lindskog, J. Mulder, C. M. Mulvey, P. Nilsson, P. Oksvold, J. Rockberg, R. Schutten, J. M. Schwenk, Å. Sivertsson, E. Sjöstedt, M. Skogs, C. Stadler, D. P. Sullivan, H. Tegel, C. Winsnes, C. Zhang, M. Zwahlen, A. Mardinoglu, F. Pontén, K. von Feilitzen, K. S. Lilley, M. Uhlén, E. Lundberg, A subcellular map of the human proteome. *Science* **356**, eaal3321 (2017). doi:10.1126/science.aal3321 Medline

52. K. G. Rothberg, J. E. Heuser, W. C. Donzell, Y.-S. Ying, J. R. Glenney, R. G. W. Anderson, Caveolin, a protein component of caveolae membrane coats. *Cell* **68**, 673–682 (1992). doi:10.1016/0092-8674(92)90143-Z Medline

53. W. Kim, E. J. Bennett, E. L. Huttlin, A. Guo, J. Li, A. Possemato, M. E. Sowa, R. Rad, J. Rush, M. J. Comb, J. W. Harper, S. P. Gygi, Systematic and quantitative assessment of the ubiquitin-modified proteome. *Mol. Cell* **44**, 325–340 (2011). doi:10.1016/j.molcel.2011.08.025 Medline

54. G. A. Wilke, J. Bubeck Wardenburg, Role of a disintegrin and metalloprotease 10 in

Staphylococcus aureus α-hemolysin–mediated cellular injury. *Proc. Natl. Acad. Sci. U.S.A.* **107**, 13473–13478 (2010). doi:10.1073/pnas.1001815107 Medline

55. I. Inoshima, N. Inoshima, G. A. Wilke, M. E. Powers, K. M. Frank, Y. Wang, J. Bubeck Wardenburg, A *Staphylococcus aureus* pore-forming toxin subverts the activity of ADAM10 to cause lethal infection in mice. *Nat. Med.* **17**, 1310–1314 (2011). doi:10.1038/nm.2451 Medline

56. E. S. Seilie, J. Bubeck Wardenburg, *Staphylococcus aureus* pore-forming toxins: The interface of pathogen and host complexity. *Semin. Cell Dev. Biol.* **72**, 101–116 (2017). doi:10.1016/j.semcdb.2017.04.003 Medline

57. J. Moreno-Càceres, L. Caja, J. Mainez, R. Mayoral, P. Martín-Sanz, R. Moreno-Vicente, M. Á. Del Pozo, S. Dooley, G. Egea, I. Fabregat, Caveolin-1 is required for TGF-β-induced transactivation of the EGF receptor pathway in hepatocytes through the activation of the metalloprotease TACE/ADAM17. *Cell Death Dis.* **5**, e1326 (2014). doi:10.1038/cddis.2014.294 Medline

58. E. M. Khan, J. M. Heidinger, M. Levy, M. P. Lisanti, T. Ravid, T. Goldkorn, Epidermal growth factor receptor exposed to oxidative stress undergoes Src- and caveolin-1-dependent perinuclear trafficking. *J. Biol. Chem.* **281**, 14486–14493 (2006). doi:10.1074/jbc.M509332200 Medline

59. M. Dal Peraro, F. G. van der Goot, Pore-forming toxins: Ancient, but never really out of fashion. *Nat. Rev. Microbiol.* **14**, 77–92 (2016). doi:10.1038/nrmicro.2015.3 Medline

60. R. Zidovetzki, I. Levitan, Use of cyclodextrins to manipulate plasma membrane cholesterol content: Evidence, misconceptions and control strategies. *Biochim. Biophys. Acta Biomembr.* **1768**, 1311–1324 (2007). doi:10.1016/j.bbamem.2007.03.026 Medline

61. Y. Wu, X. Liu, A. Akhgar, J. J. Li, H. Mok, B. R. Sellman, L. Yu, L. K. Roskos, M. T. Esser, A. Ruzin, Prevalence of IgG and neutralizing antibodies against *Staphylococcus aureus* alpha-toxin in healthy human subjects and diverse patient populations. *Infect. Immun.* **86**, e00671-17 (2018). doi:10.1128/IAI.00671-17 Medline

62. C. Gruber, D. Bogunovic, Incomplete penetrance in primary immunodeficiency: A skeleton in the closet. *Hum. Genet.* **139**, 745–757 (2020). doi:10.1007/s00439-020-02131-9 Medline

63. F. Rieux-Laucat, J. L. Casanova, Autoimmunity by haploinsufficiency. *Science* **345**, 1560–1561 (2014). doi:10.1126/science.1260791 Medline

64. H. Van Esch, P. Groenen, M. A. Nesbit, S. Schuffenhauer, P. Lichtner, G. Vanderlinden, B. Harding, R. Beetz, R. W. Bilous, I. Holdaway, N. J. Shaw, J.-P. Fryns, W. Van de Ven, R. V. Thakker, K. Devriendt, GATA3 haplo-insufficiency causes human HDR syndrome. *Nature* **406**, 419–422 (2000). doi:10.1038/35019088 Medline

65. B. Boisson, E. Laplantine, C. Dobbs, A. Cobat, N. Tarantino, M. Hazen, H. G. W. Lidov, G. Hopkins, L. Du, A. Belkadi, M. Chrabieh, Y. Itan, C. Picard, J.-C. Fournet, H. Eibel, E. Tsitsikov, S.-Y. Pai, L. Abel, W. Al-Herz, J.-L. Casanova, A. Israel, L. D. Notarangelo, Human HOIP and LUBAC deficiency underlies autoinflammation, immunodeficiency, amylopectinosis, and lymphangiectasia. *J. Exp. Med.* **212**, 939–951 (2015). doi:10.1084/jem.20141130 Medline

66. I. E. Wertz, K. M. O'Rourke, H. Zhou, M. Eby, L. Aravind, S. Seshagiri, P. Wu, C. Wiesmann, R. Baker, D. L. Boone, A. Ma, E. V. Koonin, V. M. Dixit, De-ubiquitination and ubiquitin ligase domains of A20 downregulate NF-κB signalling. *Nature* **430**, 694–699 (2004). doi:10.1038/nature02794 Medline

67. D. L. Boone, E. E. Turer, E. G. Lee, R.-C. Ahmad, M. T. Wheeler, C. Tsui, P. Hurley, M. Chien, S. Chai, O. Hitotsumatsu, E. McNally, C. Pickart, A. Ma, The ubiquitin-modifying enzyme A20 is required for termination of Toll-like receptor responses. *Nat. Immunol.* **5**, 1052–1060 (2004). doi:10.1038/ni1110 Medline

68. M. S. Ritorto, R. Ewan, A. B. Perez-Oliva, A. Knebel, S. J. Buhrlage, M. Wightman, S. M. Kelly, N. T. Wood, S. Virdee, N. S. Gray, N. A. Morrice, D. R. Alessi, M. Trost, Screening of DUB activity and specificity by MALDI-TOF mass spectrometry. *Nat. Commun.* **5**, 4763 (2014). doi:10.1038/ncomms5763 Medline

69. Q. Zhou, H. Wang, D. M. Schwartz, M. Stoffels, Y. H. Park, Y. Zhang, D. Yang, E. Demirkaya, M. Takeuchi, W. L. Tsai, J. J. Lyons, X. Yu, C. Ouyang, C. Chen, D. T. Chin, K. Zaal, S. C. Chandrasekharappa, E. P. Hanson, Z. Yu, J. C. Mullikin, S. A. Hasni, I. E. Wertz, A. K. Ombrello, D. L. Stone, P. Hoffmann, A. Jones, B. K. Barham, H. L. Leavis, A. van Royen-Kerkof, C. Sibley, E. D. Batu, A. Gül, R. M. Siegel, M. Boehm, J. D. Milner, S. Ozen, M. Gadina, J. Chae, R. M. Laxer, D. L. Kastner, I. Aksentijevich, Loss-of-function mutations in *TNFAIP3* leading to A20

70. haploinsufficiency cause an early-onset autoinflammatory disease. *Nat. Genet.* **48**, 67–73 (2016). doi:10.1038/ng.3459 Medline

70. G. R. Bignell, W. Warren, S. Seal, M. Takahashi, E. Rapley, R. Barfoot, H. Green, C. Brown, P. J. Biggs, S. R. Lakhani, C. Jones, J. Hansen, E. Blair, B. Hofmann, R. Siebert, G. Turner, D. G. Evans, C. Schrander-Stumpel, F. A. Beemer, A. van Den Ouweland, D. Halley, B. Delpech, M. G. Cleveland, I. Leigh, J. Leisti, S. Rasmussen, M. R. Wallace, C. Fenske, P. Banerjee, N. Oiso, R. Chaggar, S. Merrett, N. Leonard, M. Huber, D. Hohl, P. Chapman, J. Burn, S. Swift, A. Smith, A. Ashworth, M. R. Stratton, Identification of the familial cylindromatosis tumour-suppressor gene. *Nat. Genet.* **25**, 160–165 (2000). doi:10.1038/76006 Medline

71. P. Draber, S. Kupka, M. Reichert, H. Draberova, E. Lafont, D. de Miguel, L. Spilgies, S. Surinova, L. Taraborrelli, T. Hartwig, E. Rieser, L. Martino, K. Rittinger, H. Walczak, LUBAC-recruited CYLD and A20 regulate gene activation and cell death by exerting opposing effects on linear ubiquitin in signaling complexes. *Cell Rep.* **13**, 2258–2272 (2015). doi:10.1016/j.celrep.2015.11.009 Medline

72. P. R. Elliott, D. Leske, J. Wagstaff, L. Schlicher, G. Berridge, S. Maslen, F. Timmermann, B. Ma, R. Fischer, S. M. V. Freund, D. Komander, M. Gyrd-Hansen, Regulation of CYLD activity and specificity by phosphorylation and ubiquitin-binding CAP-Gly domains. *Cell Rep.* **37**, 109777 (2021). doi:10.1016/j.celrep.2021.109777 Medline

73. B. J. Berube, J. Bubeck Wardenburg, *Staphylococcus aureus* α-toxin: Nearly a century of intrigue. *Toxins* **5**, 1140–1166 (2013). doi:10.3390/toxins5061140 Medline

74. F. R. DeLeo, A. D. Kennedy, L. Chen, J. Bubeck Wardenburg, S. D. Kobayashi, B. Mathema, K. R. Braughton, A. R. Whitney, A. E. Villaruz, C. A. Martens, S. F. Porcella, M. J. McGavin, M. Otto, J. M. Musser, B. N. Kreiswirth, Molecular differentiation of historic phage-type 80/81 and contemporary epidemic *Staphylococcus aureus*. *Proc. Natl. Acad. Sci. U.S.A.* **108**, 18091–18096 (2011). doi:10.1073/pnas.1111084108 Medline

75. L. Stulik, S. Malafa, J. Hudcova, H. Rouha, B. Z. Henics, D. E. Craven, A. M. Sonnevend, E. Nagy, α-Hemolysin activity of methicillin-susceptible *Staphylococcus aureus* predicts ventilator-associated pneumonia. *Am. J. Respir. Crit. Care Med.* **190**, 1139–1148 (2014). doi:10.1164/rccm.201406-1012OC Medline

76. J. Bubeck Wardenburg, T. Bae, M. Otto, F. R. Deleo, O. Schneewind, Poring over pores: α-hemolysin and Panton-Valentine leukocidin in *Staphylococcus aureus* pneumonia. *Nat. Med.* **13**, 1405–1406 (2007). doi:10.1038/nm1207-1405 Medline

77. V. Thammavongsa, H. K. Kim, D. Missiakas, O. Schneewind, Staphylococcal manipulation of host immune responses. *Nat. Rev. Microbiol.* **13**, 529–543 (2015). doi:10.1038/nrmicro3521 Medline

78. A. N. Spaan, B. G. Surewaard, R. Nijland, J. A. van Strijp, Neutrophils versus *Staphylococcus aureus*: A biological tug of war. *Annu. Rev. Microbiol.* **67**, 629–650 (2013). doi:10.1146/annurev-micro-092412-155746 Medline

79. S. Y. Zhang, Herpes simplex virus encephalitis of childhood: Inborn errors of central nervous system cell-intrinsic immunity. *Hum. Genet.* **139**, 911–918 (2020). doi:10.1007/s00439-020-02127-5 Medline

80. S. Y. Zhang, O. Harschnitz, L. Studer, J. L. Casanova, Neuron-intrinsic immunity to viruses in mice and humans. *Curr. Opin. Immunol.* **72**, 309–317 (2021). doi:10.1016/j.coi.2021.07.004 Medline

81. J. L. Casanova, L. Abel, Mechanisms of viral inflammation and disease in humans. *Science* **374**, 1080–1086 (2021). doi:10.1126/science.abj7965 Medline

82. F. Galbiati, B. Razani, M. P. Lisanti, Emerging themes in lipid rafts and caveolae. *Cell* **106**, 403–411 (2001). doi:10.1016/S0092-8674(01)00472-X Medline

83. S. D. Conner, S. L. Schmid, Regulated portals of entry into the cell. *Nature* **422**, 37–44 (2003). doi:10.1038/nature01451 Medline

84. E. Tacconelli, E. Carrara, A. Savoldi, S. Harbarth, M. Mendelson, D. L. Monnet, C. Pulcini, G. Kahlmeter, J. Kluytmans, Y. Carmeli, M. Ouellette, K. Outterson, J. Patel, M. Cavaleri, E. M. Cox, C. R. Houchens, M. L. Grayson, P. Hansen, N. Singh, U. Theuretzbacher, N. Magrini; WHO Pathogens Priority List Working Group, Discovery, research, and development of new antibiotics: The WHO priority list of antibiotic-resistant bacteria and tuberculosis. *Lancet Infect. Dis.* **18**, 318–327 (2018). doi:10.1016/S1473-3099(17)30753-3 Medline

85. B. François, H. S. Jafri, J. Chastre, M. Sánchez-García, P. Eggimann, P.-F. Dequin, V. Huberlant, L. Viña Soria, T. Boulain, C. Bretonnière, J. Pugin, J. Trenado, A. C. Hernandez Padilla, O. Ali, K. Shoemaker, P. Ren, F. E. Coenjaerts, A. Ruzin, O.

Barraud, L. Timbermont, C. Lammens, V. Pierre, Y. Wu, J. Vignaud, S. Colbert, T. Bellamy, M. T. Esser, F. Dubovsky, M. J. Bonten, H. Goossens, P.-F. Laterre; COMBACTE Consortium and the SAATELLITE Study Group, Efficacy and safety of suvratoxumab for prevention of *Staphylococcus aureus* ventilator-associated pneumonia (SAATELLITE): A multicentre, randomised, double-blind, placebo-controlled, parallel-group, phase 2 pilot trial. *Lancet Infect. Dis.* **21**, 1313–1323 (2021). doi:10.1016/S1473-3099(20)30995-6 Medline

86. W. Salgado-Pabón, P. M. Schlievert, Models matter: The search for an effective *Staphylococcus aureus* vaccine. *Nat. Rev. Microbiol.* **12**, 585–591 (2014). doi:10.1038/nrmicro3308 Medline

87. M. von Köckritz-Blickwede, M. Rohde, S. Oehmcke, L. S. Miller, A. L. Cheung, H. Herwald, S. Foster, E. Medina, Immunological mechanisms underlying the genetic predisposition to severe *Staphylococcus aureus* infection in the mouse model. *Am. J. Pathol.* **173**, 1657–1668 (2008). doi:10.2353/ajpath.2008.080337 Medline

88. F. Randow, J. D. MacMicking, L. C. James, Cellular self-defense: How cell-autonomous immunity protects against pathogens. *Science* **340**, 701–706 (2013). doi:10.1126/science.1233028 Medline

89. R. G. Gaudet, S. Zhu, A. Halder, B.-H. Kim, C. J. Bradfield, S. Huang, D. Xu, A. Mamiñska, T. N. Nguyen, M. Lazarou, E. Karatekin, K. Gupta, J. D. MacMicking, A human apolipoprotein L with detergent-like activity kills intracellular pathogens. *Science* **373**, eabf8113 (2021). doi:10.1126/science.abf8113 Medline

90. C. Nathan, Rethinking immunology. *Science* **373**, 276–277 (2021). doi:10.1126/science.abj5637 Medline

91. A. N. Spaan, J. A. G. van Strijp, V. J. Torres, Leukocidins: Staphylococcal bi-component pore-forming toxins find their receptors. *Nat. Rev. Microbiol.* **15**, 435–447 (2017). doi:10.1038/nrmicro.2017.27 Medline

92. H. Rouha, A. Badarau, Z. C. Visram, M. B. Battles, B. Prinz, Z. Magyarics, G. Nagy, I. Mirkina, L. Stulik, M. Zerbs, M. Jägerhofer, B. Maierhofer, A. Teubenbacher, I. Dolezilkova, K. Gross, S. Banerjee, G. Zauner, S. Malafa, J. Zmajkovic, S. Maier, R. Mabry, E. Krauland, K. D. Wittrup, T. U. Gerngross, E. Nagy, Five birds, one stone: Neutralization of α-hemolysin and 4 bi-component leukocidins of *Staphylococcus aureus* with a single human monoclonal antibody. *mAbs* **7**, 243–254 (2015). doi:10.4161/19420862.2014.985132 Medline

93. S. Belkaya, A. R. Kontorovich, M. Byun, S. Mulero-Navarro, F. Bajolle, A. Cobat, R. Josowitz, Y. Itan, R. Quint, L. Lorenzo, S. Boucherit, C. Stoven, S. Di Filippo, L. Abel, S.-Y. Zhang, D. Bonnet, B. D. Gelb, J.-L. Casanova, Autosomal recessive cardiomyopathy presenting as acute myocarditis. *J. Am. Coll. Cardiol.* **69**, 1653–1665 (2017). doi:10.1016/j.jacc.2017.01.043 Medline

94. S. Y. Zhang, N. E. Clark, C. A. Freije, E. Pauwels, A. J. Taggart, S. Okada, H. Mandel, P. Garcia, M. J. Ciancanelli, A. Biran, F. G. Lafaille, M. Tsumura, A. Cobat, J. Luo, S. Volpi, B. Zimmer, S. Sakata, A. Dinis, O. Ohara, E. J. Garcia Reino, K. Dobbs, M. Hasek, S. P. Holloway, K. McCammon, S. A. Hussong, N. DeRosa, C. E. Van Skike, A. Katolik, L. Lorenzo, M. Hyodo, E. Faria, R. Halwani, R. Fukuhara, G. A. Smith, V. Galvan, M. J. Damha, S. Al-Muhsen, Y. Itan, J. D. Boeke, L. D. Notarangelo, L. Studer, M. Kobayashi, L. Diogo, W. G. Fairbrother, L. Abel, B. R. Rosenberg, P. J. Hart, A. Etzioni, J.-L. Casanova, Inborn errors of RNA lariat metabolism in humans with brainstem viral infection. *Cell* **172**, 952–965.e18 (2018). doi:10.1016/j.cell.2018.02.019 Medline

95. S. Belkaya, E. Michailidis, C. B. Korol, M. Kabbani, A. Cobat, P. Bastard, Y. S. Lee, N. Hernandez, S. Drutman, Y. P. de Jong, E. Vivier, J. Bruneau, V. Béziat, B. Boisson, L. Lorenzo-Diaz, S. Boucherit, M. Sebagh, E. Jacquemin, J.-F. Emile, L. Abel, C. M. Rice, E. Jouanguy, J.-L. Casanova, Inherited IL-18BP deficiency in human fulminant viral hepatitis. *J. Exp. Med.* **216**, 1777–1790 (2019). doi:10.1084/jem.20190669 Medline

96. R. Yang, F. Mele, L. Worley, D. Langlais, J. Rosain, I. Benhsaien, H. Elarabi, C. A. Croft, J.-M. Doisne, P. Zhang, M. Weisshaar, D. Jarrossay, D. Latorre, Y. Shen, J. Han, M. Ogishi, C. Gruber, J. Markle, F. Al Ali, M. Rahman, T. Khan, Y. Seeleuthner, G. Kerner, L. T. Husquin, J. L. MacIsaac, M. Jeljeli, A. Errami, F. Ailal, M. S. Kobor, C. Oleaga-Quintas, M. Roynard, M. Bourgey, J. El Baghdadi, S. Boisson-Dupuis, A. Puel, F. Batteux, F. Rozenberg, N. Marr, Q. Pan-Hammarström, D. Bogunovic, L. Quintana-Murci, T. Carroll, C. S. Ma, L. Abel, A. Bousfiha, J. P. Di Santo, L. H. Glimcher, P. Gros, S. G. Tangye, F. Sallusto, J. Bustamante, J.-L. Casanova, Human T-bet governs innate and innate-like adaptive IFN-γ immunity against mycobacteria. *Cell* **183**, 1826–1847.e31 (2020). doi:10.1016/j.cell.2020.10.046 Medline

97. M. K. Hospenthal, T. E. T. Mevissen, D. Komander, Deubiquitinase-based analysis of ubiquitin chain architecture using Ubiquitin Chain Restriction (UbiCRest). *Nat. Protoc.* **10**, 349–361 (2015). doi:10.1038/nprot.2015.018 Medline

98. S. Bolte, F. P. Cordelières, A guided tour into subcellular colocalization analysis in light microscopy. *J. Microsc.* **224**, 213–232 (2006). doi:10.1111/j.1365-2818.2006.01706.x Medline

99. A. Ruzin, Y. Wu, L. Yu, X.-Q. Yu, D. E. Tabor, H. Mok, C. Tkaczyk, K. Jensen, T. Bellamy, L. Roskos, M. T. Esser, H. S. Jafri, Characterisation of anti-alpha toxin antibody levels and colonisation status after administration of an investigational human monoclonal antibody, MEDI4893, against *Staphylococcus aureus* alpha toxin. *Clin. Transl. Immunology* **7**, e1009 (2018). doi:10.1002/cti2.1009 Medline

100. S. Anders, P. T. Pyl, W. Huber, HTSeq—A Python framework to work with high-throughput sequencing data. *Bioinformatics* **31**, 166–169 (2015). doi:10.1093/bioinformatics/btu638 Medline

101. T. Baslan, J. Kendall, K. Volyanskyy, K. McNamara, H. Cox, S. D'Italia, F. Ambrosio, M. Riggs, L. Rodgers, A. Leotta, J. Song, Y. Mao, J. Wu, R. Shah, R. Gularte-Mérida, K. Chadalavada, G. Nanjangud, V. Varadan, A. Gordon, C. Curtis, A. Krasnitz, N. Dimitrova, L. Harris, M. Wigler, J. Hicks, Novel insights into breast cancer copy number genetic heterogeneity revealed by single-cell genome sequencing. *eLife* **9**, e51480 (2020). doi:10.7554/eLife.51480 Medline

102. J. Cox, M. Mann, MaxQuant enables high peptide identification rates, individualized p.p.b.-range mass accuracies and proteome-wide protein quantification. *Nat. Biotechnol.* **26**, 1367–1372 (2008). doi:10.1038/nbt.1511 Medline

103. B. A. Diep, S. R. Gill, R. F. Chang, T. H. V. Phan, J. H. Chen, M. G. Davidson, F. Lin, J. Lin, H. A. Carleton, E. F. Mongodin, G. F. Sensabaugh, F. Perdreau-Remington, Complete genome sequence of USA300, an epidemic clone of community-acquired meticillin-resistant *Staphylococcus aureus*. *Lancet* **367**, 731–739 (2006). doi:10.1016/S0140-6736(06)68231-7 Medline

104. G. Dittmar, K. F. Winklhofer, Linear ubiquitin chains: Cellular functions and strategies for detection and quantification. *Front Chem.* **7**, 915 (2020). doi:10.3389/fchem.2019.00915 Medline

105. A. Dobin, C. A. Davis, F. Schlesinger, J. Drenkow, C. Zaleski, S. Jha, P. Batut, M. Chaisson, T. R. Gingeras, STAR: Ultrafast universal RNA-seq aligner. *Bioinformatics* **29**, 15–21 (2013). doi:10.1093/bioinformatics/bts635 Medline

106. A. K. Dreyer, D. Hoffmann, N. Lachmann, M. Ackermann, D. Steinemann, B. Timm, U. Siler, J. Reichenbach, M. Grez, T. Moritz, A. Schambach, T. Cathomen, TALEN-mediated functional correction of X-linked chronic granulomatous disease in patient-derived induced pluripotent stem cells. *Biomaterials* **69**, 191–200 (2015). doi:10.1016/j.biomaterials.2015.07.057 Medline

107. H. Guet-Revillet, H. Coignard-Biehler, J.-P. Jais, G. Quesne, E. Frapy, S. Poirée, A.-S. Le Guern, A. Le Flèche-Matéos, A. Hovnanian, P.-H. Consigny, O. Lortholary, X. Nassif, A. Nassif, O. Join-Lambert, Bacterial pathogens associated with hidradenitis suppurativa, France. *Emerg. Infect. Dis.* **20**, 1990–1998 (2014). doi:10.3201/eid2012.140064 Medline

108. O. Join-Lambert, H. Coignard-Biehler, J.-P. Jais, M. Delage, H. Guet-Revillet, S. Poirée, S. Duchatelet, V. Jullien, A. Hovnanian, O. Lortholary, X. Nassif, A. Nassif, Efficacy of ertapenem in severe hidradenitis suppurativa: A pilot study in a cohort of 30 consecutive patients. *J. Antimicrob. Chemother.* **71**, 513–520 (2016). doi:10.1093/jac/dkv361 Medline

109. M. D. Keller, K. L. Ching, F.-X. Liang, A. Dhabaria, K. Tam, B. M. Ueberheide, D. Unutmaz, V. J. Torres, K. Cadwell, Decoy exosomes provide protection against bacterial toxins. *Nature* **579**, 260–264 (2020). doi:10.1038/s41586-020-2066-6 Medline

110. H. Li, R. Durbin, Fast and accurate short read alignment with Burrows-Wheeler transform. *Bioinformatics* **25**, 1754–1760 (2009). doi:10.1093/bioinformatics/btp324 Medline

111. H. Li, B. Handsaker, A. Wysoker, T. Fennell, J. Ruan, N. Homer, G. Marth, G. Abecasis, R. Durbin; 1000 Genome Project Data Processing Subgroup, The Sequence Alignment/Map format and SAMtools. *Bioinformatics* **25**, 2078–2079 (2009). doi:10.1093/bioinformatics/btp352 Medline

112. M. I. Love, W. Huber, S. Anders, Moderated estimation of fold change and dispersion for RNA-seq data with DESeq2. *Genome Biol.* **15**, 550 (2014). doi:10.1186/s13059-014-0550-8 Medline

113. A. McKenna, M. Hanna, E. Banks, A. Sivachenko, K. Cibulskis, A. Kernytsky, K.

Garimella, D. Altshuler, S. Gabriel, M. Daly, M. A. DePristo, The Genome Analysis Toolkit: A MapReduce framework for analyzing next-generation DNA sequencing data. *Genome Res.* **20**, 1297–1303 (2010). doi:10.1101/gr.107524.110 Medline

114. S. Mishra, A. R. Horswill, Heparin mimics extracellular DNA in binding to cell surface-localized proteins and promoting *Staphylococcus aureus* biofilm formation. *MSphere* **2**, e00135-17 (2017). doi:10.1128/mSphere.00135-17 Medline

115. S. Tyanova, T. Temu, P. Sinitcyn, A. Carlson, M. Y. Hein, T. Geiger, M. Mann, J. Cox, The Perseus computational platform for comprehensive analysis of (prote)omics data. *Nat. Methods* **13**, 731–740 (2016). doi:10.1038/nmeth.3901 Medline

116. J. J. Velarde, M. O'Seaghdha, B. Baddal, B. Bastiat-Sempe, M. R. Wessels, Binding of NAD⁺-glycohydrolase to streptolysin O stabilizes both toxins and promotes virulence of group A *Streptococcus*. *mBio* **8**, e01382-17 (2017). doi:10.1128/mBio.01382-17 Medline

117. S. Virreira Winter, A. Zychlinsky, B. W. Bardoel, Genome-wide CRISPR screen reveals novel host factors required for *Staphylococcus aureus* α-hemolysin-mediated toxicity. *Sci. Rep.* **6**, 24242 (2016). doi:10.1038/srep24242 Medline

118. D. Wessel, U. I. Flügge, A method for the quantitative recovery of protein in dilute solution in the presence of detergents and lipids. *Anal. Biochem.* **138**, 141–143 (1984). doi:10.1016/0003-2697(84)90782-6 Medline

119. D. Zhang, J. W. Pridgeon, P. H. Klesius, Expression and activity of recombinant proaerolysin derived from *Aeromonas hydrophila* cultured from diseased channel catfish. *Vet. Microbiol.* **165**, 478–482 (2013). doi:10.1016/j.vetmic.2013.04.023 Medline

120. G. X. Zheng, J. M. Terry, P. Belgrader, P. Ryvkin, Z. W. Bent, R. Wilson, S. B. Ziraldo, T. D. Wheeler, G. P. McDermott, J. Zhu, M. T. Gregory, J. Shuga, L. Montesclaros, J. G. Underwood, D. A. Masquelier, S. Y. Nishimura, M. Schnall-Levin, P. W. Wyatt, C. M. Hindson, R. Bharadwaj, A. Wong, K. D. Ness, L. W. Beppu, H. J. Deeg, C. McFarland, K. R. Loeb, W. J. Valente, N. G. Ericson, E. A. Stevens, J. P. Radich, T. S. Mikkelsen, B. J. Hindson, J. H. Bielas, Massively parallel digital transcriptional profiling of single cells. *Nat. Commun.* **8**, 14049 (2017). doi:10.1038/ncomms14049 Medline

121. I. Korsunsky, N. Millard, J. Fan, K. Slowikowski, F. Zhang, K. Wei, Y. Baglaenko, M. Brenner, P. R. Loh, S. Raychaudhuri, Fast, sensitive and accurate integration of single-cell data with Harmony. *Nat. Methods* **16**, 1289–1296 (2019). doi:10.1038/s41592-019-0619-0 Medline

122. N. Lachmann, M. Ackermann, E. Frenzel, S. Liebhaber, S. Brennig, C. Happle, D. Hoffmann, O. Klimenkova, D. Lüttge, T. Buchegger, M. P. Kühnel, A. Schambach, S. Janciauskiene, C. Figueiredo, G. Hansen, J. Skokowa, T. Moritz, Large-scale hematopoietic differentiation of human induced pluripotent stem cells provides granulocytes or macrophages for cell replacement therapies. *Stem Cell Reports* **4**, 282–296 (2015). doi:10.1016/j.stemcr.2015.01.005 Medline

123. M. Ogishi, R. Yang, C. Aytekin, D. Langlais, M. Bourgey, T. Khan, F. A. Ali, M. Rahman, O. M. Delmonte, M. Chrabieh, P. Zhang, C. Gruber, S. J. Pelham, A. N. Spaan, J. Rosain, W.-T. Lei, S. Drutman, M. D. Hellmann, M. K. Callahan, M. Adamow, P. Wong, J. D. Wolchok, G. Rao, C. S. Ma, Y. Nakajima, T. Yaguchi, K. Chamoto, S. C. Williams, J.-F. Emile, F. Rozenberg, M. S. Glickman, F. Rapaport, G. Kerner, G. Allington, I. Tezcan, T. Cagdas, F. O. Hosnut, F. Dogu, A. Ikinciogullari, V. K. Rao, L. Kainulainen, V. Béziat, J. Bustamante, S. Vilarinho, R. P. Lifton, B. Boisson, L. Abel, D. Bogunovic, N. Marr, L. D. Notarangelo, S. G. Tangye, T. Honjo, P. Gros, S. Boisson-Dupuis, J.-L. Casanova, Inherited PD-1 deficiency underlies tuberculosis and autoimmunity in a child. *Nat. Med.* **27**, 1646–1654 (2021). doi:10.1038/s41591-021-01388-5 Medline

124. S. Tarazona, P. Furió-Tarí, D. Turrà, A. D. Pietro, M. J. Nueda, A. Ferrer, A. Conesa, Data quality aware analysis of differential expression in RNA-seq with NOISeq R/Bioc package. *Nucleic Acids Res.* **43**, e140 (2015). doi:10.1093/nar/gkv711 Medline

125. M. Akkurt Arslan, I. Kolman, C. Pionneau, S. Chardonnet, R. Magny, C. Baudouin, F. Brignole-Baudouin, K. Kessal, Proteomic analysis of tears and conjunctival cells collected with Schirmer strips using timsTOF Pro: Preanalytical considerations. *Metabolites* **12**, 2 (2021). doi:10.3390/metabo12010002 Medline

126. O. Langella, B. Valot, T. Balliau, M. Blein-Nicolas, L. Bonhomme, M. Zivy, X!TandemPipeline: A tool to manage sequence redundancy for protein inference and phosphosite identification. *J. Proteome Res.* **16**, 494–503 (2017). doi:10.1021/acs.jproteome.6b00632 Medline

127. B. MacLean, D. M. Tomazela, N. Shulman, M. Chambers, G. L. Finney, B. Frewen, R. Kern, D. L. Tabb, D. C. Liebler, M. J. MacCoss, Skyline: An open source document editor for creating and analyzing targeted proteomics experiments. *Bioinformatics* **26**, 966–968 (2010). doi:10.1093/bioinformatics/btq054 Medline

128. A. Shevchenko, H. Tomas, J. Havli, J. V. Olsen, M. Mann, In-gel digestion for mass spectrometric characterization of proteins and proteomes. *Nat. Protoc.* **1**, 2856–2860 (2006). doi:10.1038/nprot.2006.468 Medline

ACKNOWLEDGMENTS

SUPPLEMENTARY MATERIALS

science.org/doi/10.1126/science.abm6380
Case Reports for the Patients Studied
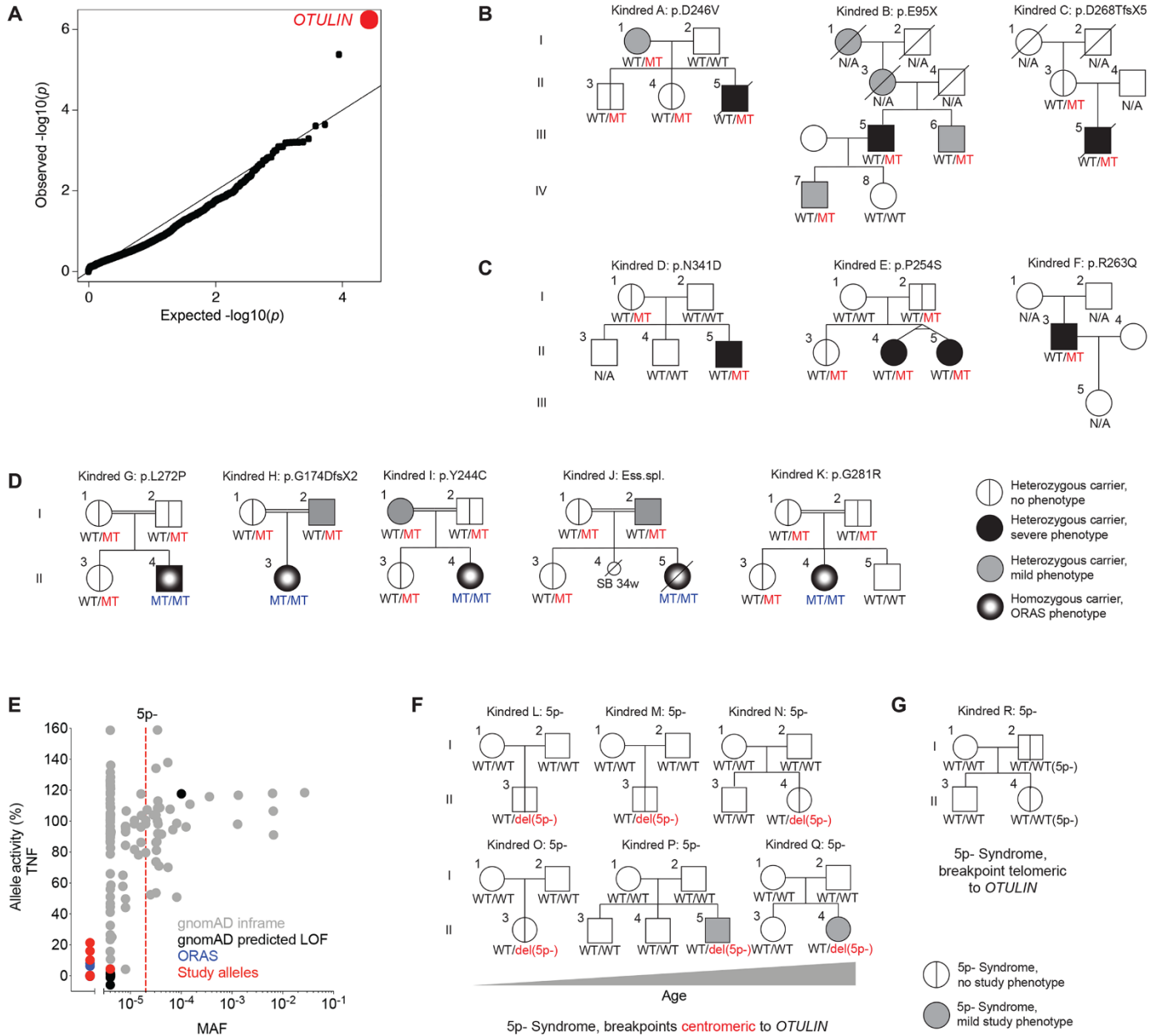Materials and Methods
Figs. S1 to S7
Tables S1 to S4
References (*100–128*)
MDAR Reproducibility Checklist

Submitted 30 September 2021; accepted 5 May 2022
Published online 19 May 2022
10.1126/science.abm6380

Fig. 1. OTULIN haploinsufficiency and its molecular characterization. (**A**) Genome-wide enrichment in rare, predicted deleterious variants in the cohort of N = 105 patients with severe staphylococcal disease, relative to N = 1,274 patients with mycobacterial disease. (**B**) Pedigrees of the kindreds presenting severe necrotizing staphylococcal disease and carrying heterozygous mutations of *OTULIN*. (**C**) Pedigrees of the kindreds carrying heterozygous mutations of *OTULIN* and presenting necrosis triggered by other etiologies. (**D**) Pedigrees of the kindreds of ORAS probands carrying biallelic mutations of *OTULIN*. (**E**) Functional population genetics based on minor allele frequencies (MAFs) reported in the gnomAD database and the NF-κB inhibitory capacity of the OTULIN variants, as assessed with a luciferase reporter system in transiently transfected HEK293T cells stimulated with TNF (datapoints represent the mean of N = 4-5 per variant). (**F**) Pedigrees of the kindreds of the 5p- syndrome probands carrying deletions with a breakpoint centromeric to *OTULIN*. The patients are shown in ascending age order (left to right, top to bottom). (**G**) Pedigree of the 5p- syndrome kindred with probands carrying a deletion with a breakpoint telomeric to *OTULIN*. WT: wild-type allele; MT: mutant allele; LOF: loss of function. See also fig. S1 and tables S1 and S2.
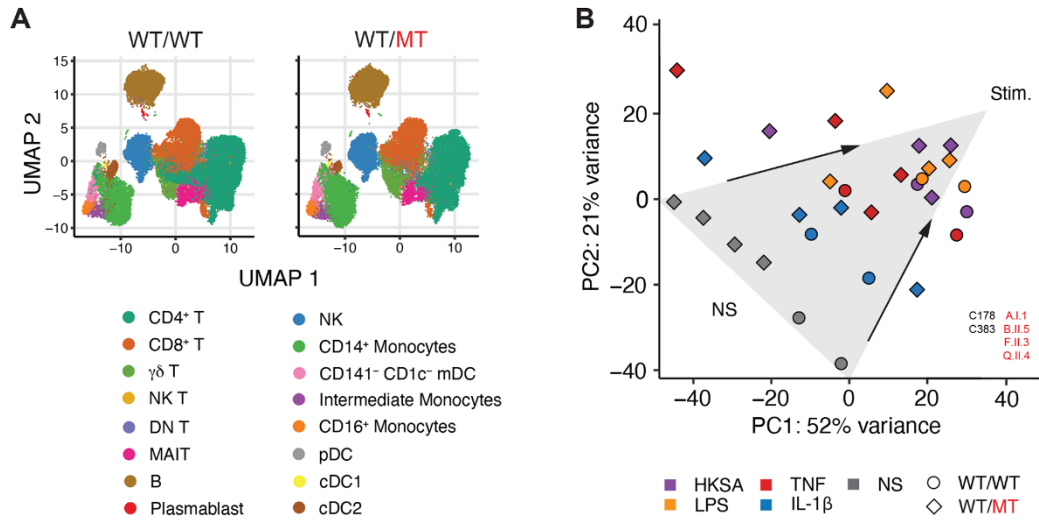
Fig. 2. OTULIN haploinsufficiency does not impair the hematopoietic immune system. (A) Aggregate uniform manifold approximation and projection (UMAP) plots of peripheral blood mononuclear cells (PBMCs) from patients with autosomal dominant OTULIN deficiency and healthy controls, as assessed by cytometry by time-of-flight (CyTOF). (B) Principal component (PC) analysis plot of the transcriptional profile of PBMCs at baseline and after incubation with various stimuli, in comparison with healthy controls. Arrows have been added for visual support of the direction of variance after stimulation. NS: not stimulated; HKSA: heat-killed *S. aureus*. See also fig. S2.
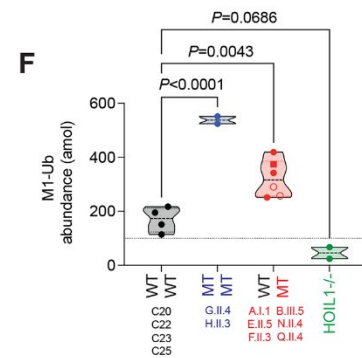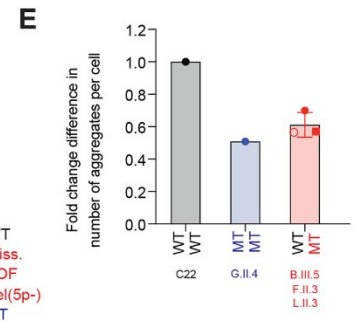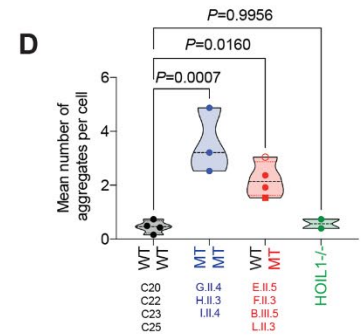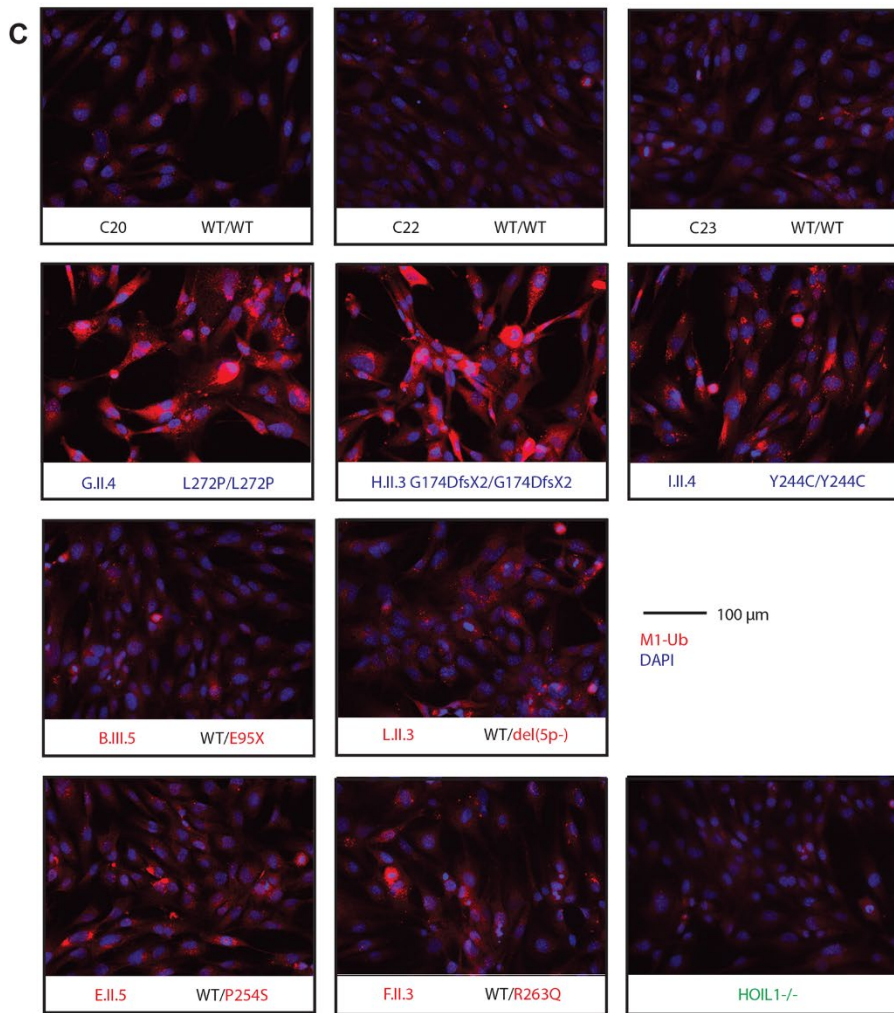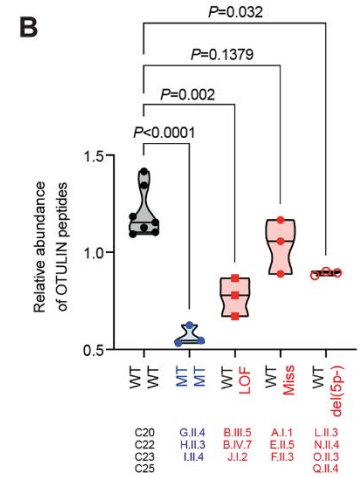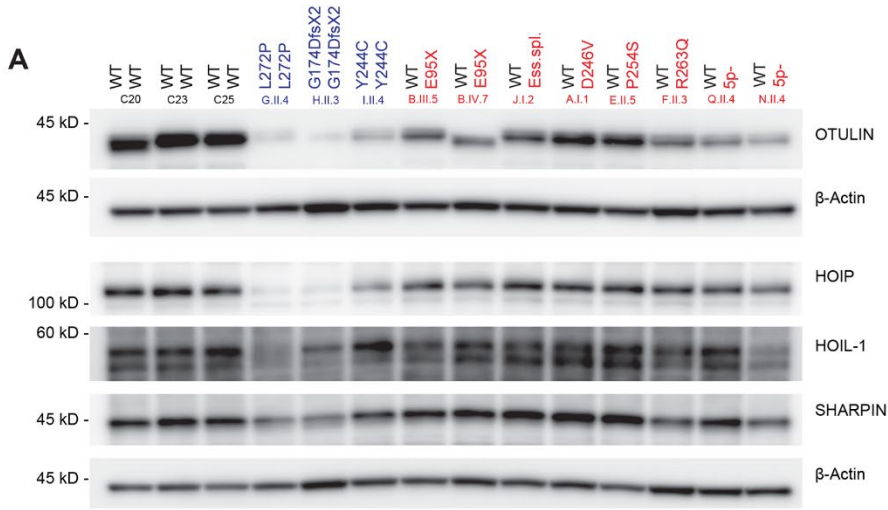
Fig. 3. *OTULIN* gene dosage-dependent accumulation of M1-Ub in fibroblasts. (**A**) Expression of OTULIN, HOIP, HOIL-1, and SHARPIN in primary dermal fibroblasts (PDFs). (**B**) Relative abundance of OTULIN peptides in PDFs, as determined by mass spectrometry analysis (median). (**C**) Accumulation of aggregates containing M1-Ub in immortalized fibroblasts, as assessed by immunohistochemistry. Representative images. (**D**) Quantification of the aggregate accumulations seen in (D) (median). (**E**) Quantification of aggregates containing M1-Ub in immortalized fibroblasts after rescue with wild-type OTULIN, as compared with cells rescued with an empty virus (mean ±SD). (**F**) Abundance of M1-Ub, as determined by AQUA-MS/MS analysis of immortalized fibroblasts (median). Statistical significance was calculated by ANOVA with Dunnett post hoc correction for multiple comparisons. See also fig. S3.
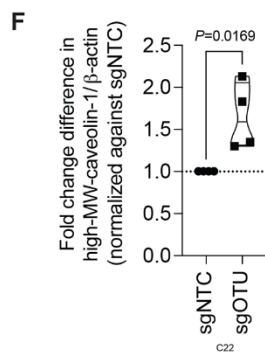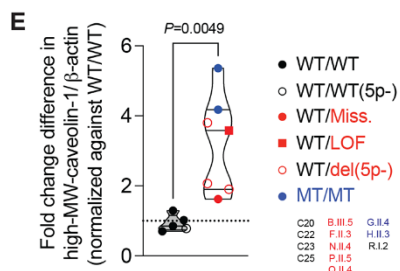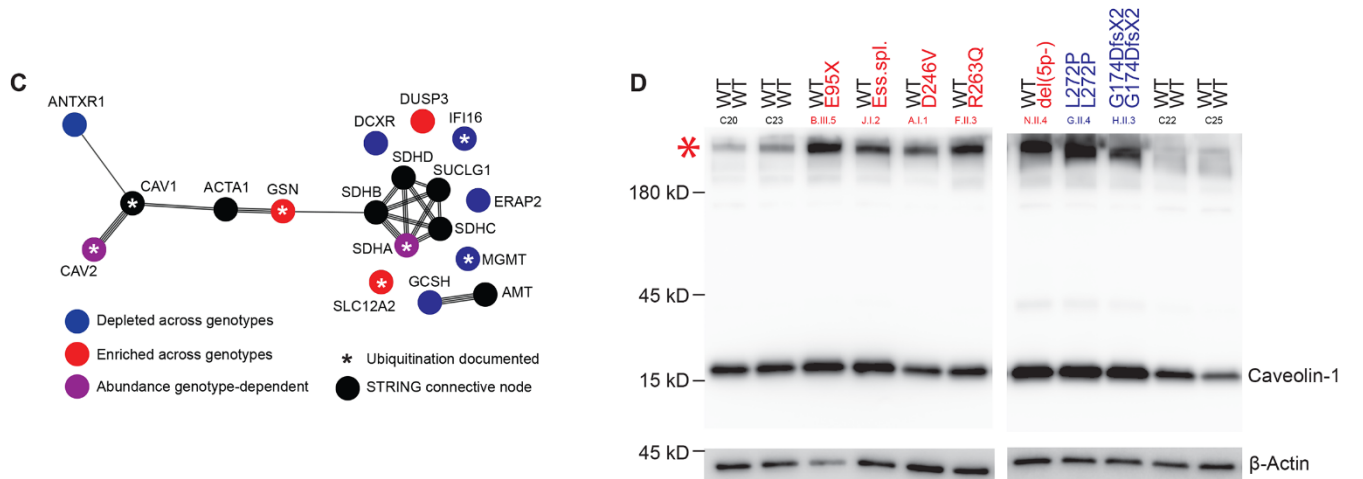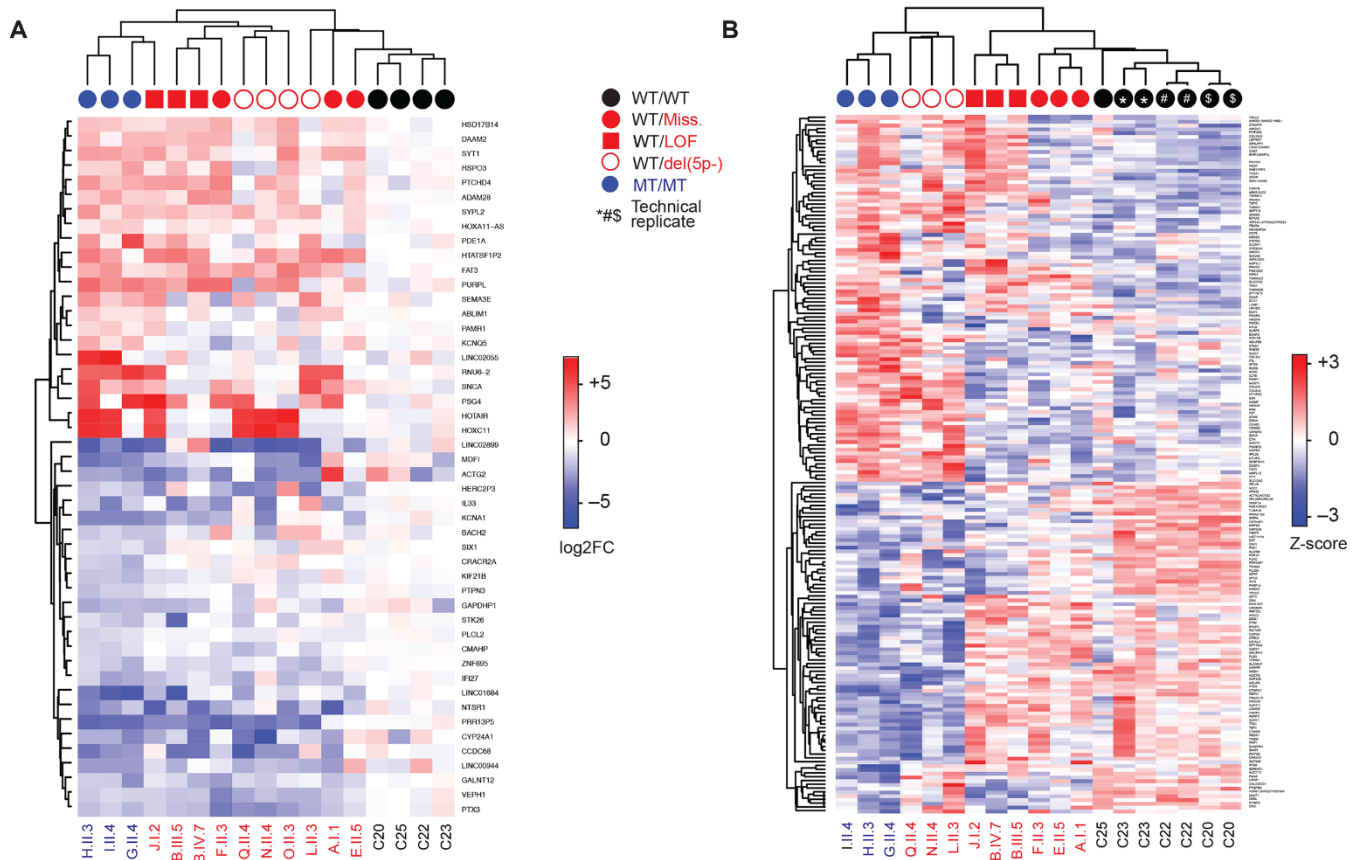
Fig. 4. *OTULIN*-dependent accumulation of caveolin-1 in fibroblasts. (**A**) Transcriptional profile of unstimulated primary dermal fibroblasts (PDFs), as assessed by RNA sequencing, expressed as $\log_2$-fold changes (FC) relative to the mean value for controls. Genes satisfying the threshold for statistical significance in comparisons of ORAS patients to controls are shown. (**B**) Proteomic profiles of unstimulated PDFs, as assessed by mass spectrometry on whole-cell lysates, expressed as Z-scores. Genes satisfying the threshold for statistical significance in comparisons of ORAS patients to controls are shown. (**C**) STRING analysis of the cluster of proteins with differential abundances in various genotypes identified in (B). (**D**) Accumulation of SDS-resistant high-MW caveolin-1-containing complexes in PDF-whole cell lysates (WCLs). (**E**) High-MW caveolin-1-containing complex intensities relative to β-actin intensities in PDF-WCLs, normalized against the mean value of healthy controls (datapoints indicate the mean of $N = 2$ replicates per patient, median per group). (**F**) High-MW caveolin-1-containing complex intensities relative to β-actin intensities in PDF-WCLs treated with an sgRNA pool targeting *OTULIN* (sgOTU), normalized against the mean value in those treated with a non-targeting control sgRNA (sgNTC) (median, $N = 4$). The statistical significance of differences was assessed in Student's *t*-tests. See also fig. S4.
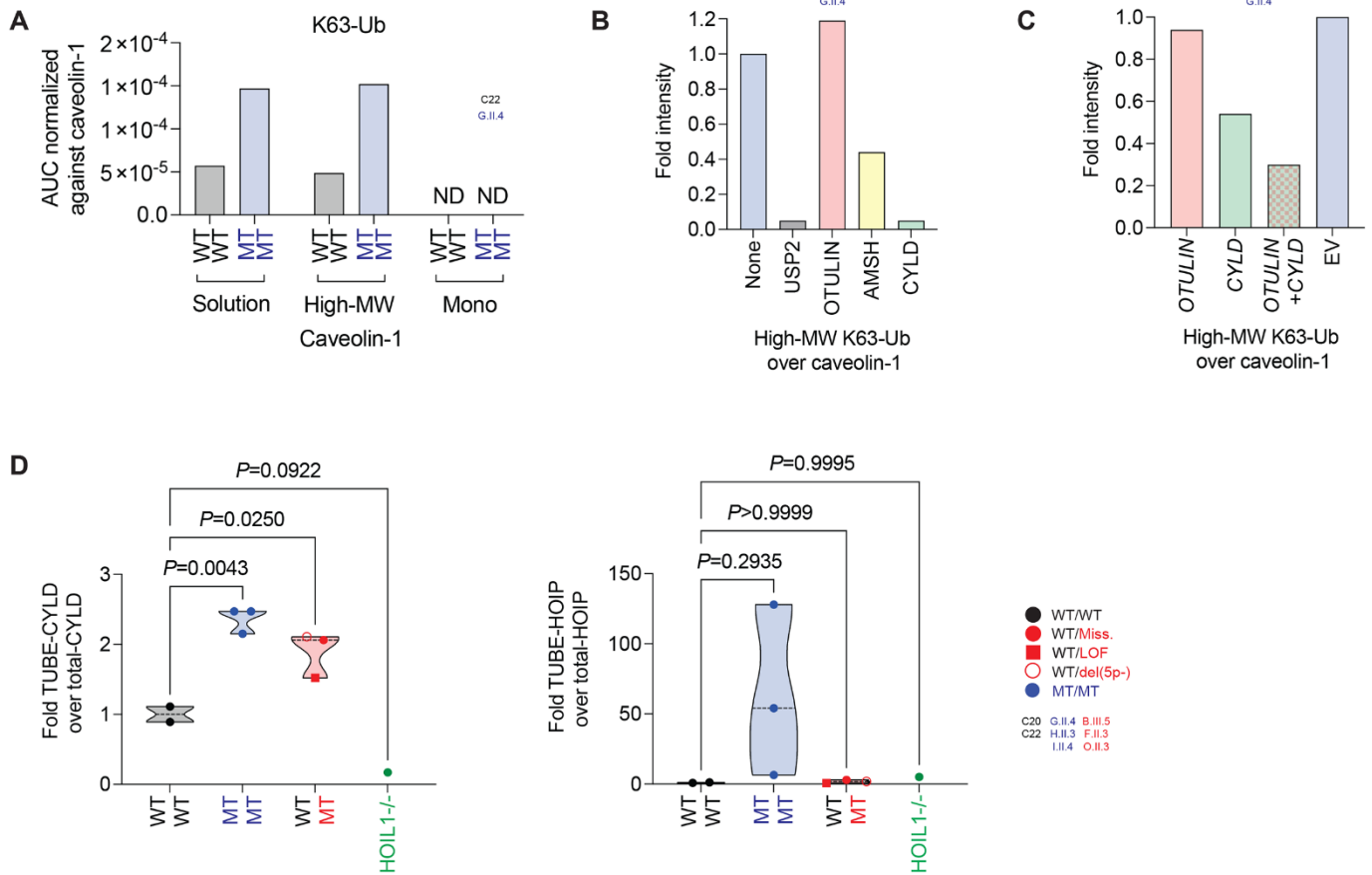
Fig. 5. Polyubiquitination of caveolin-1. (**A**) Analysis of K63-Ub on caveolin-1 by LC-MS/MS on purified caveolin-1 from primary dermal fibroblast (PDF) whole cell lysates (WCLs). Caveolin-1 was analyzed in solution, in the high-molecular weight (MW) complex fraction, and in the monomeric (Mono) fraction. (**B**) High-MW K63-Ub complex intensities relative to caveolin-1 intensities in recombinant deubiquitinase-treated purified caveolin-1 from PDFs. (**C**) High-MW K63-Ub complex intensities relative to caveolin-1 intensities in purified caveolin-1 from PDFs after rescue with *CYLD* and/or *OTULIN*. (**D**) Intensities of CYLD and HOIP bound to M1-Ub, as detected in TUBE pull-downs from immortalized fibroblasts, relative to intensities of total CYLD and HOIP, respectively. Statistical significance was calculated by ANOVA with Dunnett post hoc correction for multiple comparisons. See also fig. S5.
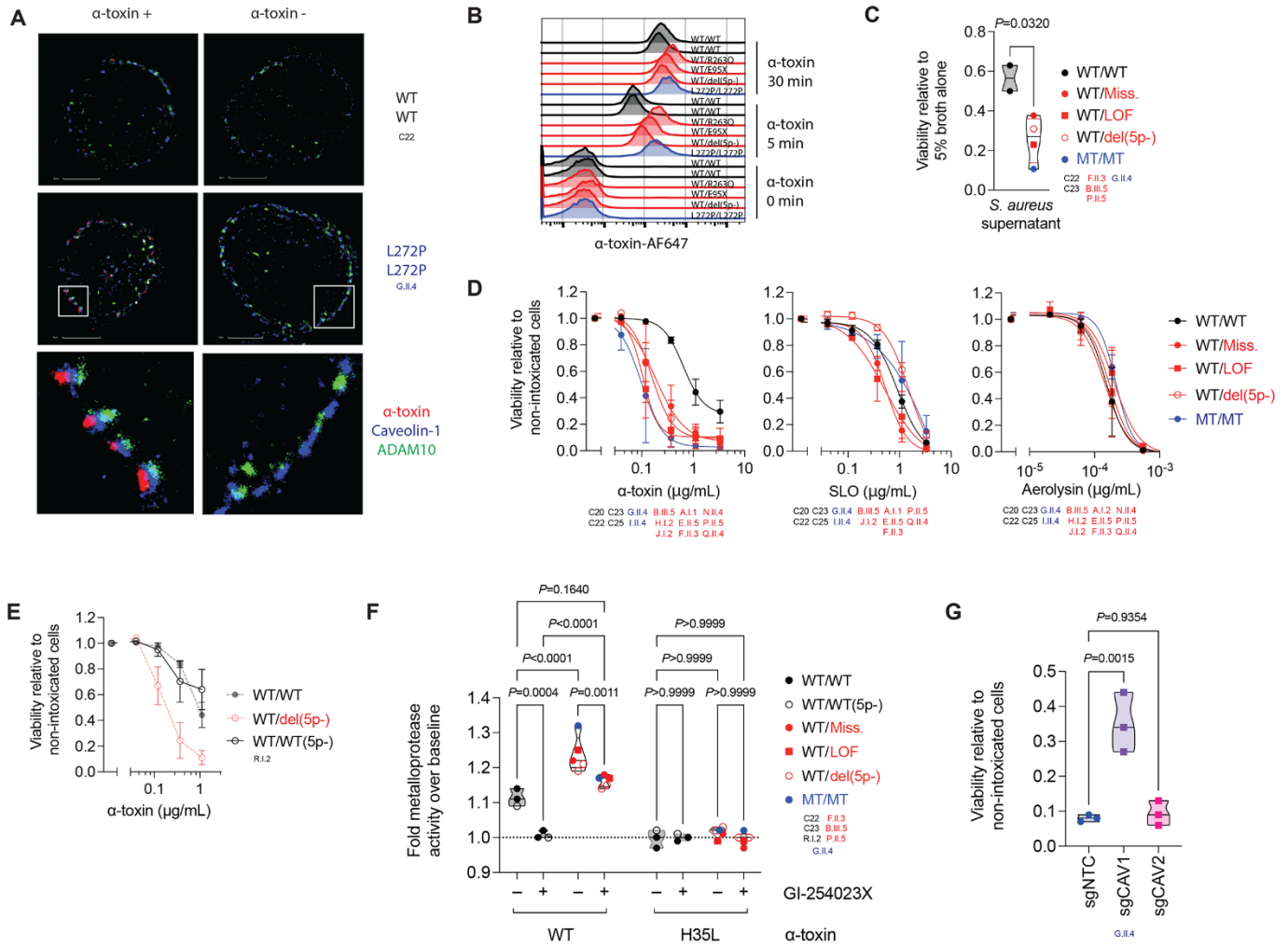
Fig. 6. OTULIN haploinsufficiency impairs intrinsic immunity to α-toxin in fibroblasts. (**A**) Colocalization of α-toxin with ADAM10 and caveolin-1 in primary dermal fibroblasts (PDFs), visualized in high-resolution images acquired by stochastic optical reconstruction microscopy, after 30 min of incubation in the presence or absence of α-toxin. (**B**) Binding of α-toxin in PDFs, as detected by flow cytometry. (**C**) Viability of PDFs following 2.5 hours of incubation with culture supernatant from *S. aureus* (datapoints indicate the mean of *N* = 3 replicates per patient, median per group). (**D**) Viability of PDFs following 24 hours of incubation with recombinant microbial toxins (*N* = 2-4 per group, mean ±SD per group). (**E**) Viability of PDFs from a 5p- syndrome patient with a breakpoint telomeric to *OTULIN* following 24 hours of incubation with recombinant α-toxin, superimposed on that for healthy controls and 5p- patients with a breakpoint centromeric to *OTULIN* from panel (F) (*N* = 3, mean ±SD). (**F**) Cell-surface metalloprotease activity in PDFs induced by wild type α-toxin (WT) or a toxoid mutant (H35L) following the treatment of cells with an ADAM10 inhibitor or carrier (datapoints indicate the mean of *N* = 3 replicates per patient, median per group). (**G**) Viability of OTULIN-deficient PDFs treated with an sgRNA pool targeting *CAV1* (sgCAV1), *CAV2* (sgCAV2), or a non-targeting control sgRNA (sgNTC) following exposure to α-toxin (0.12 μg/ml; *N* = 3, median). The statistical significance of differences was assessed in Student's *t*-tests (C), or by ANOVA with Bonferroni (F) or Dunnett (G) post hoc corrections for multiple comparisons. See also fig. S6.
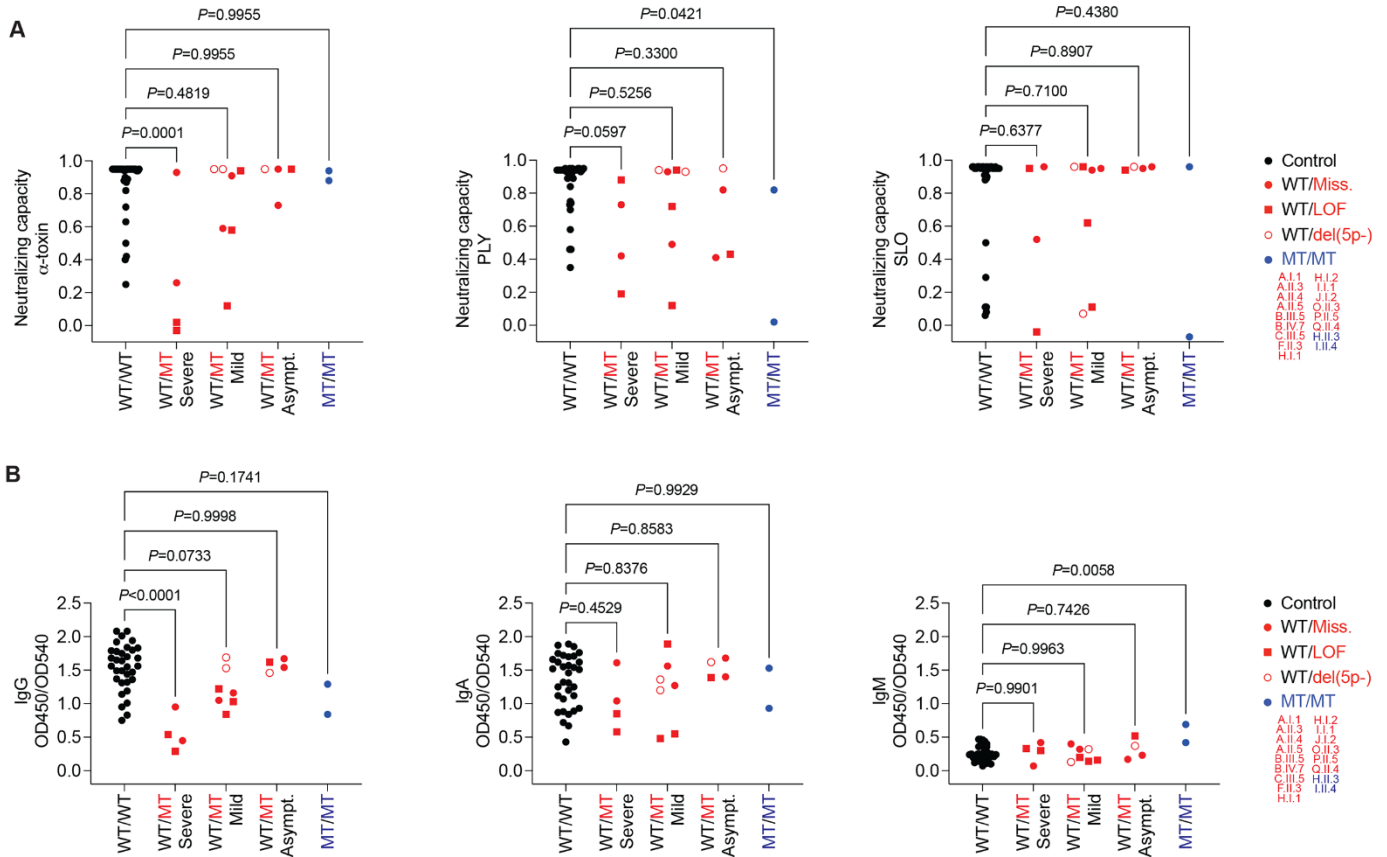
Fig. 7. α-Toxin-neutralizing antibodies rescue OTULIN haploinsufficiency. (A) Capacity of plasma at a dilution of 1:300 to neutralize the hemolytic activity of α-toxin (20 ng/ml), pneumolysin (PLY, 0.67 ng/ml), and streptolysin O (SLO, 42 ng/ml) in rabbit erythrocytes. **(B)** Anti-α-toxin immunoglobulin levels in plasma at a dilution of 1:750. We analyzed plasma from adult patients, relatives, and controls. The statistical significance of differences was determined by ANOVA with Dunnett post hoc correction for multiple comparisons. See also fig. S7.